Energy Methods and Finite Element Analysis in Orthodontic Applications

A Thesis

Presented in Partial Fulfillment of the Requirements for the

Degree of Master of Science

with a

Major in Mechanical Engineering

in the

College of Graduate Studies

University of Idaho

by

Sarah A. Willis

Major Professor: Edwin Odom, Ph.D.

Committee Members: Steven Beyerlein, Ph.D.; Richard Nielsen, Ph.D.

Department Administrator: Steven Beyerlein, Ph.D.

May 2019

Authorization to Submit Thesis

This thesis of Sarah A. Willis, submitted for the degree of Master of Science with a Major in Mechanical Engineering and titled "Energy Methods and Finite Element Analysis in Orthodontic Applications" has been reviewed in final form. Permission, as indicated by the signatures and dates below, is now granted to submit final copies to the College of Graduate Studies for approval.

Major Professor:	_____ Edwin Odom, Ph.D.	Date: _____
Committee Members:	_____ Steven Beyerlein, Ph.D.	Date: _____
	_____ Richard Nielsen, Ph.D.	Date: _____
Department Administrator:	_____ Steven Beyerlein, Ph.D.	Date: _____

Abstract

The purpose of this research was to verify, using finite element analysis, a proposed closed-form solution which solved for the reaction forces on a patient's teeth during orthodontic treatment.

The results were verified by constructing a progressive series of models in Abaqus and comparing the calculated displacements to their closed-form solutions. The final orthodontic model featured a nickel-titanium archwire subjected to the fourteen reaction forces obtained from the proposed closed-form solution. Elastic and plastic behavior was considered through use of a bilinear model. The displacements obtained from the FEA model were compared to the actual displacements measured between the start and end positions of the patient's teeth.

The difference between the closed-form and FEA in the elastic regime was negligible. The values at the location of the largest discrepancy still matched to the fourth decimal place. The graphs of displacement obtained from the closed-form and FEA solutions overlapped each other. Additionally, the deformed shape of the archwire produced analytically and numerically was very similar in the plastic regime.

The results of this research are the validation of the closed-form solution using a modified form of Castigliano's Theorem, as well as the establishment and visual representation of the relationship between applied force and orthodontic displacement.

Acknowledgements

I would like to acknowledge Dr. Edwin Odom, Dr. Frederick Ju, Dr. Steve Beyerlein, Dr. Richard Nielsen, Dr. Rezaie, Dr. Potirniche, Dr. Maughan, Dr. Crepeau, Dr. Stephens, Bill Magnie, Dr. Humes, all of the students I taught, Schweitzer Engineering Laboratories, Nightforce Optics, and the University of Idaho Mechanical Engineering Department.

Dedication

For my mother, Paula, and my father, William.

Table of Contents

List of Figures

Chapter 1: Introduction

This research was built on the goal to model and solve for reaction forces in an orthodontic force system. Simply, the question to be answered was: how much force does the orthodontic archwire apply to a patient's teeth during orthodontic treatment? All that is known to help answer this question is information regarding the positions of a patient's teeth and the hardware used to correct dental alignment.

There are two components in an orthodontic force system which will be discussed. There are the brackets, which are the metal components glued to the patient's teeth, and the archwire. Both are shown in Figure 1-1.

Figure 1-1 Orthodontic Hardware

Source: Adapted from [1]

The brackets are stationary relative to the teeth. The archwire slides through the brackets. The archwire is composed of a memory shape alloy and is manufactured in an elliptical shape as shown in Figure 1-2.

Figure 1-2 Orthodontic Archwires

Source: Adapted from [2]

The archwire is bent and trimmed as needed to roughly fit the crooked arrangement of the patient's teeth. It is then guided through each of the brackets. Over time, the memory shape alloy of the archwire returns to its original form, taking the teeth with it. However, there is no information on the force it takes to move each of those teeth to a more desirable position. There has been no study conducted to provide insight as to what is the force on each of a patient's teeth during orthodontic treatment.

A closed-form solution to solve for the reaction forces as a system was developed by Dr. Edwin Odom. The solution utilized the original and final positions of the patient's teeth to determine the displacement of each tooth. These displacement values were used in a modified form of Castigliano's theorem along with the Crotti-Engesser method to solve a system of 14 equations for the unknowns: 14 reaction forces.

Castigliano's theorem is most commonly applied to linear-elastic beams in bending. The theorem relates a force magnitude to the deflection at point of force application through the partial derivative of the strain energy.

The Crotti-Engesser theory extends from Castigliano's theorem to include inelastic deformation through the use of complimentary energy. This theory uses a relationship between curvature and bending moment. The literature on the applications of the Crotti-Engesser theory to a complex model is sparse. There is a need to verify the theory and to verify that the orthodontic math model was accurate.

The work done for graduate research consisted of developing secondary means of validating the proposed closed-form solution. The chosen method was finite element analysis. Before proceeding to create a finite element model of the final orthodontic model, a series of base cases were developed. The purpose of the base cases was to be able to verify that the FEA models and mathematical methods were accurate. For the some of the base cases, a published solution already exists. This was used as a tool for comparison against the FEA and closed-form solutions. The base cases started with elastic beams featuring various end conditions which were analyzed using Castigliano's theorem and FEA. The base cases progressed to include inelastic material behavior by utilizing the complimentary energy with the Crotti-Engesser theory and FEA. The analysis did not include unloading for these problems. The base cases concluded with beams featuring curved geometry. From there, the final orthodontic model was developed.

For the finite element analysis, the orthodontic system was modeled as an elliptical archwire with 14 forces applied at the locations where the patient's teeth would be located. After the finite element analysis was completed, the mathematical model developed using the modified form of Castigliano's theorem and the Crotti-Engesser theory was verified. This was accomplished by comparing the displacements at point of force application obtained from the finite element program to the actual displacements of the patient's teeth.

Literature Search

Castigliano's theorem relates a point load to the displacement at that load through the partial derivative of the strain energy. It is often used to compute deflections in structures. The theorem was developed Carlo Alberto Castigliano and published in 1879 [3]. It has been successfully applied to multiple mechanics problems to solve for deflection in components. For examples, see the fifth chapter of *Advanced Mechanics of Materials* [4]. There are two theorems encompassed in Castigliano's principle of minimum strain energy. The first theorem states that a force magnitude can be solved for by taking the partial derivative of the strain energy with respect to the displacement caused by that force. The second theorem states that a displacement can be solved for by taking the partial derivative of the strain energy with respect to the point load causing that displacement. The general form of Castigliano's theorem in terms of the strain energy of bending is:

$$\delta_i = \frac{\partial U}{\partial F_i} = \int_o^L \frac{M}{EI}\frac{\partial M_i}{\partial F_i}dx$$

The strain energy is designated by U. The terms F_i and δ_i are the applied force and displacement at some location i. M is the moment, E is the elastic modulus, and I is the moment of inertia. The theorem is commonly applied to statically determinate structures. The application of Castigliano's theorem to statically indeterminate structures with other types of supports, including pin or roller connections is more complex.

Dr. Frederick Ju [5], a professor of Mechanical Engineering at the University of New Mexico, proposed a modified form of Castigliano's theorem which could be applied to a broader scope of problems. This modified form is presented below.

$$\delta_i = \int_o^L \frac{M}{EI}\frac{\partial M_i}{\partial F_i}dx + \lambda_i \frac{\partial g_n}{\partial F_i}$$

Dr. Ju's method of using Castigliano's theorem involved the addition of some constant(s), $\lambda_i \frac{\partial g_n}{\partial F_i}$, where λ_i is a Lagrange multiplier and $\frac{\partial g_n}{\partial F_i}$ is the partial derivative of an equation of equilibrium. These components act as constraints that account for various supports of the system. By using Castigliano's theorem with Lagrange multipliers, one can relate forces and displacements on components that do not have a fixed end condition or are statically indeterminate. Utilizing this form of Castigliano's theorem will allow the solution of more complex problems. Dr. Ju published his methods in his paper, *On the Constraints of Castigliano's Theorem*. [5] This paper

has been referenced four times. The most recent of these references utilized Dr. Ju's method to solve for reaction forces caused by friction in a statically indeterminate curved beam. [6] The next two sources were published by Dr. Edwin Odom, the major professor on this presented thesis and research and his colleague, Dr. Carla Egelhoff. The papers reported on using Dr. Ju's method to solve for deflections in statically determinate stepped shafts and solving for deflection in stepped shafts using energy methods and numerical integration at an undergraduate level. [7] [8] The last of the four citations proposed using Castigliano's Theorem to model the flexibility of robotic manipulator arms. [9] Dr. Ju's initial article is the only known proposal on altering Castigliano's theorem such that in can be applied to a broader scope of problems. The application of this method to something as complex as an orthodontic force system has not been published.

Chapter 2: Castigliano's Theorem and its Limitations

Introduction

This chapter will introduce the mathematics, principles and theory in detail that support this research. Castigliano's theorem and its limitations will be discussed. Additionally, this chapter presents methods to modify the theorem such that it can be applied to the problems presented in this thesis. The chapter will conclude by describing the finite element analysis. It will discuss the material properties, the type of finite element model, and the other necessary aspects of finite element analysis.

Methods and Materials

Math Model

The mathematical model for the orthodontic force system was developed on the concept of Castigliano's theorem. Castigliano's theorem relates a deflection to a load through the partial derivative of the strain energy.

$$\delta_i = \frac{\partial U}{\partial F_i} \tag{2-1}$$

Here, U is the internal strain energy, δ_i is the deflection at location i in the direction of the load, F_i. This equation in terms of bending strain energy is shown below.

$$\delta_i = \int_o^L \frac{M}{EI}\frac{\partial M_i}{\partial F_i} dx \tag{2-2}$$

In Equation (2-2), M is the moment as a function of x, E is the elastic modulus, I is the moment of inertia and $\frac{\partial M_i}{\partial F_i}$ is the partial derivative of the moment equation with respect to the point load applied where the deflection, δ_i, is of interest. This method is commonly applied to cantilevered beams, as demonstrated in Figure 2-1.

The right end of the beam features an unyielding support. The variable x is taken toward the fixed end, such that integration can be performed over the length of the beam and the deflection at the application of load P can be determined.

Figure 2-1 Standard Energy Method Problem

However, a typical orthodontic force system does not involve unyielding supports. The orthodontic archwire is threaded through the brackets (the components glued to the patient's teeth), and is permitted to slide axially, more like a roller support. For the orthodontic model, there were fourteen of these supports. Refer to Figure 2-2 for clarity.

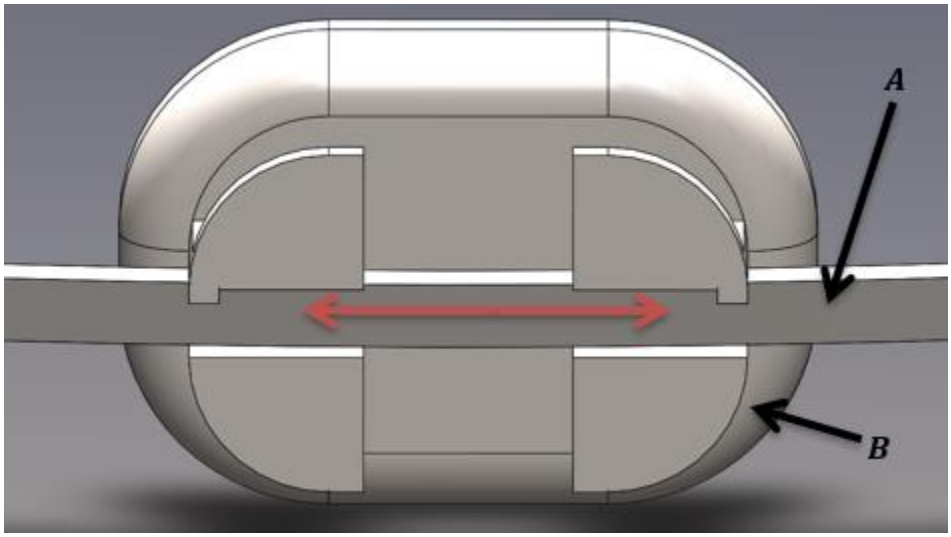

Figure 2-2 Archwire (A) and Bracket (B)

Equation (2-2) applies to instances with unyielding supports or instances involving statically determinate beams. For the orthodontic force system, a modified version of Castigliano's theorem had to be utilized. Dr. Frederick Ju proposed the use of Lagrange multipliers in addition to Equation (2-2) in order to account for the other end conditions when integration is not performed away from a free end toward an unyielding support. When including Lagrange multipliers, the equation becomes:

$$\delta_i = \int_o^L \frac{M}{EI}\frac{\partial M_i}{\partial F_i}dx + \lambda_i \frac{\partial g_n}{\partial F_i} \tag{2-3}$$

Here, λ_i is the Lagrange multiplier associated with g_n, an equation of equilibrium. The example below shows how Castigliano's theorem represented by Equation (2-2) has limitations when the equations of equilibrium are not considered. The example then shows how this can be accounted for using the modified form of Castigliano's theorem represented by Equation (2-3).

For example, consider the simply supported beam with a uniformly distributed load shown in Figure 2-3.

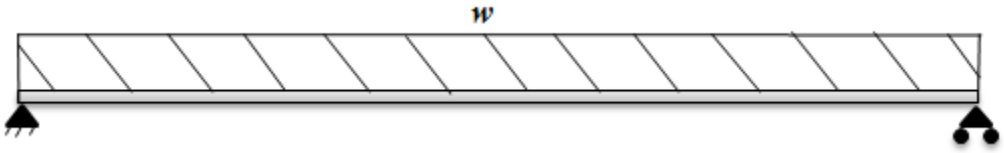

Figure 2-3Simply Supported Beam with Distributed Load

The free body diagram for the beam is shown in Figure 2-4.

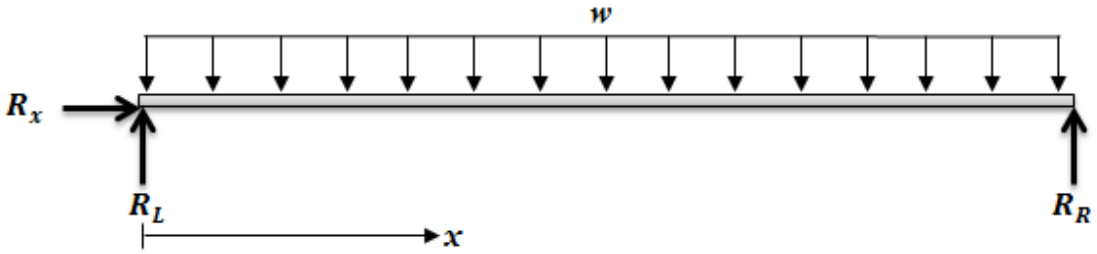

Figure 2-4 Free Body Diagram

Note that the reaction force R_x arises from the pinned connection at the left end. However, as the only load acting in the x-direction, the value of R_x is zero.

The moment equation is formed and shown below.

$$M(x) = R_L x - \frac{wx^2}{2}$$

Now, the goal will be to use the zero-displacement conditions at the ends of the beam and Castigliano's theorem without the constraints of the equations of equilibrium to determine the values for R_L and R_R. Essentially, Equation (2-2) will be used to back-solve for the reaction forces since the deflection at the end of the beam is already known to be zero. The partial derivative of the moment with respect to the load R_L is:

$$\frac{\partial M}{\partial R_L} = x$$

The moment equation and the partial derivative are used in Equation (2-2) as shown below.

$$\delta_L = \int_o^L \frac{R_L x - \frac{wx^2}{2}}{EI} x\, dx$$

Using the zero-displacement condition at the left end of the beam, the equation simplifies as shown below. The EI term is constant and can be pulled outside the integral.

$$0 = \frac{1}{EI}\int_o^L RLx^2 - \frac{wx^3}{2} dx$$

By multiplying both sides by *EI* and integrating with respect to *x*, the equation becomes:

$$0 = \frac{RLx^3}{3} - \frac{wx^4}{8}\Big|_0^L$$

After evaluating the equation between the bounds of integration, R_L is solved for.

$$R_L = \frac{3wL}{8}$$

This is incorrect. One can look at the free body diagram above and understand that the correct value for R_L is:

$$R_L = \frac{wL}{2}$$

The reason that applying Castigliano's theorem to this case was unsuccessful is because the problem involves a roller and a pin instead of a completely fixed end and a free end.

Now this problem will be solved for the displacement along the length of the beam using the modified version of Castigliano's theorem represented by Equation (2-3) to produce a closed-form solution. The closed-form solution obtained using this method will be compared to the published closed-form solution found in most mechanics textbooks. The true support conditions of this problem are taken into account in the form of Lagrange multipliers.

In Figures 2-5 and 2-6, it must be noted that *Q* is a fictitious or imaginary load with a true value of zero. The force, *Q*, is present so the deflection can be determined at every point along the beam as the location of *Q* moves along the length of the beam. By definition, Castigliano's theorem solves for deflection at the point of load application. There must be a load present where deflection is to be determined, even if the actual value of that load is zero.

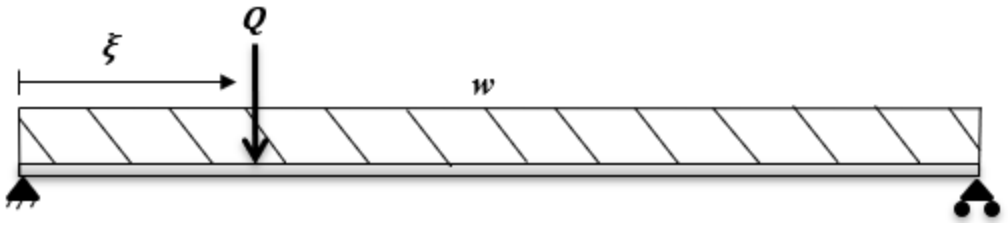

Figure 2-5 Simply Supported Beam with Fictitious Load

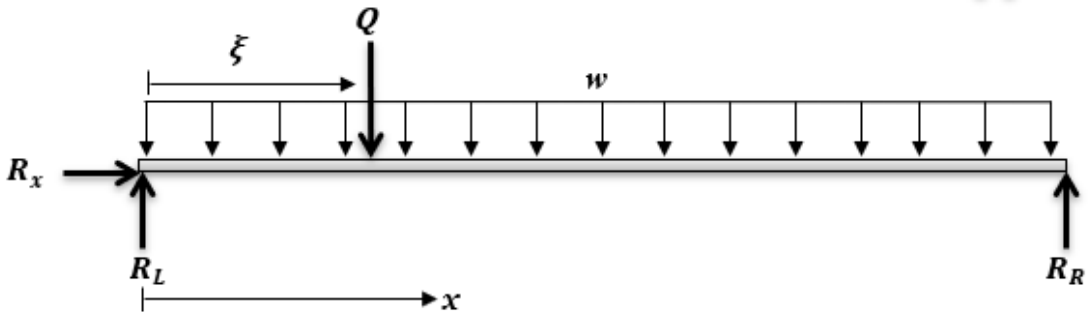

Figure 2-6 Free Body Diagram Including Fictitious Load

To start the process of solving the previous problem using this modified method, the equations of equilibrium must be determined. The sum of the forces is taken in the *y*-direction, and is denoted as g_1.

$$g_1 = \sum F_y = 0 = R_L + R_R - Q - wL$$

Next, the sum of the moments is taken about the right end of the beam. This will be denoted g_2.

$$g_2 = \sum M_R = 0 = R_L(L) - Q(x - \xi) - \frac{1}{2}wL^2$$

Moving in the direction of x, the moment equation is formed and is shown below. Note the Heaviside step function included. This simply means that for H(a,b), if b>a then the Heaviside function evaluates to the value of 1, and the function f(a,b) will be present in the equation. However, if b<a, then the Heaviside function evaluates to zero, and the function f(a,b) will not be present in the equation, as it is multiplied by zero.

$$M(x) = R_L x - Q(x - \xi) * H(x, \xi) - \frac{wx^2}{2}$$

Following Professor Ju's approach for g_1, it is seen that the force R_R is implicit in the moment equation, meaning it does not appear in the moment equation. Additionally, the displacement

caused by R_R is zero, meaning the force R_R is also non-working. Therefore, g_1 is ignorable, and there will not be a Lagrange multiplier associated with it. But looking at g_2, it is seen that R_L, Q, and w all appear in the moment equation, $M(x)$, making them explicit variables in the moment equation. This means g_2 is an explicit constraint and cannot be ignored and there will be a Lagrange multiplier associated. This Lagrange multiplier must first be determined in order to solve for displacement along the length of the beam. The left end of the beam has a zero-displacement condition. Equation (2-3) will be used as shown below.

$$\delta_L = \int \frac{M}{EI}\frac{\partial M}{\partial R_L}dx + \lambda_2 \frac{\partial g_2}{\partial R_L}$$

The moment equation and partial derivatives are shown in the equation:

$$0 = \int_0^L \frac{R_L x - \frac{wx^2}{2}}{EI} * x dx + \lambda_2 L$$

After integrating and multiplying out the EI term, the equation becomes:

$$0 = \frac{R_L L^3}{3} - \frac{wL^4}{8} + \lambda_2 EIL$$

Recall from equation g_1 that R_L is equal to $\frac{wL}{2}$. This will be used to simplify the equation further.

$$0 = \frac{wL^4}{6} - \frac{wL^4}{8} + \lambda_2 EIL$$

The Lagrange multiplier, λ_2, can now be determined.

$$\lambda_2 = -\frac{wL^3}{24EI}$$

Next, the integral to solve for deflection along the entire length of the beam can be constructed. Note that the equation takes the form of Equation (2-3). The partial derivatives in the equation are now with respect to the load Q.

$$\frac{\partial U}{\partial Q} = \delta_Q = \int_0^L \frac{R_L x - \frac{wx^2}{2}}{EI} * -(x-\xi) * H(x,\xi) dx + \lambda_2 * \big(-(L-\xi)\big)$$

The bounds of integration can be adjusted to account for the Heaviside step function. When the value of x is between zero and ξ, the Heaviside step function will evaluate to zero. For x values between ξ and L, the Heaviside function evaluates to one. Therefore, the lower bound of

integration can be replaced by ξ and the Heaviside function dropped. The *EI* term can be multiplied out to form the following equation.

$$\delta_Q EI = \int_{\xi}^{L} \left(R_L x - \frac{wx^2}{2} \right) * \big(-(x-\xi)\big) dx - \lambda_2 EI(L-\xi)$$

After integration and evaluation between the bounds, the equation becomes:

$$EI\delta_Q = \left(\frac{L^4 w}{8} - \frac{R_L L^3}{3} - \frac{L^3 w\xi}{6} + \frac{R_L L^2 \xi}{2} + \frac{w\xi^4}{24} - \frac{R_L \xi^3}{6} \right) - \lambda_2 EI(L-\xi)$$

After combining like terms, and including the value for λ_2, the displacement at any point Q on the beam is represented by Equation (2-4).

$$\delta_Q = \frac{w\xi}{24EI}(L^3 - 2L\xi^2 - \xi^3) \tag{2-4}$$

This is the closed-form solution for the displacement along the length of the beam. This can be validated using the closed-form solution of the moment-curvature relationship is presented in *Mechanical Engineering Design.* [10]

$$y = \frac{wx}{24EI}(2Lx^2 - x^3 - L^3) \tag{2-5}$$

The only difference that can be seen between the published solution represented by Equation (2-5), and Equation (2-4) is a negative sign that has been distributed to all the terms in the parentheses in Equation (2-5). This is because the published solution was developed on the assumption that the distributed load is acting in the negative *y*-direction. But Castigliano's theorem relates a displacement to a point load *in the direction of the point load*. Therefore, the sign is dictated by the force.

It was shown that the correct solution to this problem was not produced using the general form of Castigliano's theorem alone. It was shown that the value for the Lagrange multiplier needed to be included in order to produce the correct solution.

Nonlinear Behavior

The geometry of the orthodontic force system was not the only problem presented when applying Castigliano's theorem to this problem. Aside from dealing with the types of supports present in the orthodontic system, the other issue addressed was the inelastic deformation experienced by the archwire during orthodontic treatment. Castigliano's second

theorem is only applicable when stresses and displacements occur in the linear elastic region. The generalized form of Castigliano's theorem represented by Equation (2-2) no longer applies to the non-linear bending of the archwire. This is because the relationship between strain energy, applied force and displacement changes to complementary energy, applied force and displacement. In Figure 2-7, the strain energy is represented as U, and the complementary energy is denoted U_c. In the linear region, $U=U_c$. However, once the curve moves past the yield point and into the non-linear regime, $U \neq U_c$. When non-linear stress is experienced, the complementary energy, U_c must be used in place of U. The general equation becomes:

$$\delta_i = \frac{\partial U_c}{\partial F_i} \tag{2-6}$$

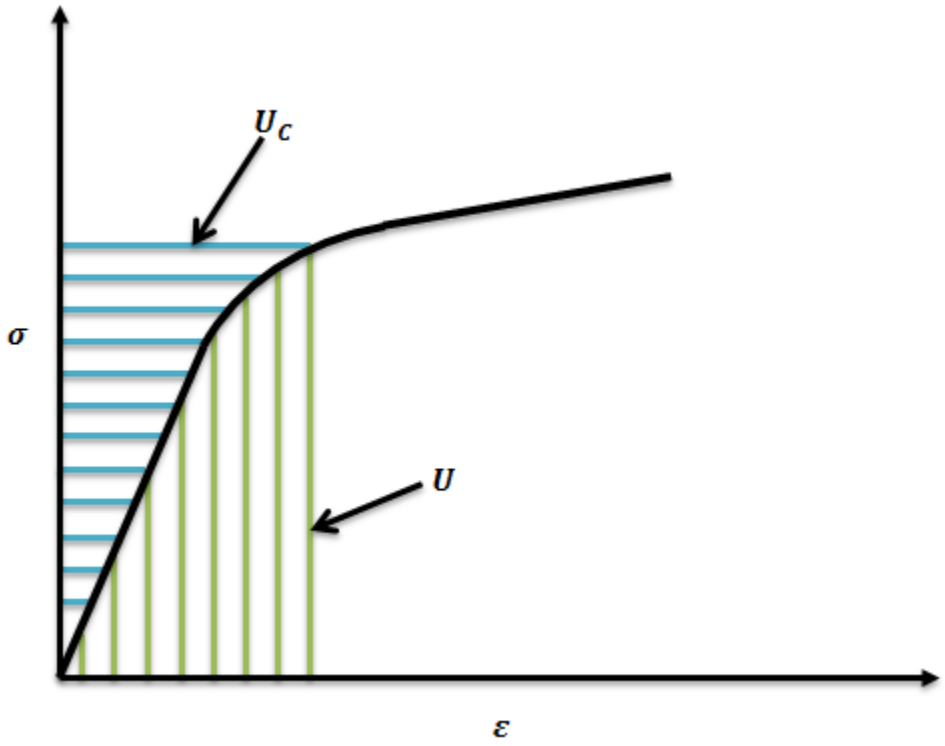

Figure 2-7 Strain and Complementary Energy

Assuming Euler-Bernoulli behavior, planes before bending remain plane after bending as shown in Figure 2-8.

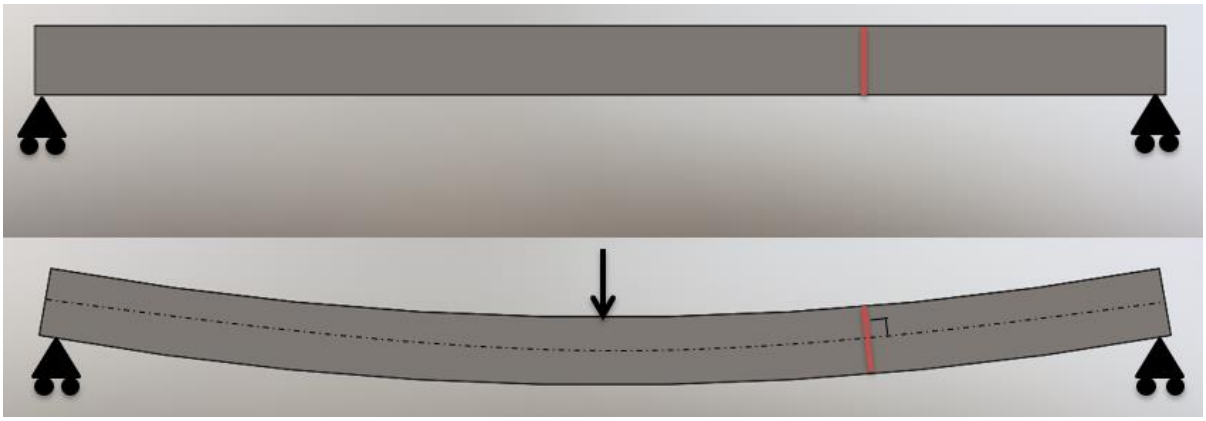

Figure 2-8 Eulerian Beam Theory

After the material exceeds the yield strain, the stress profile is no longer linear as shown in Figure 2-10 (a). However, the strain distribution is linear as shown in Figure 2-10 (b).

Figure 2-9 Cross Section in Inelastic Bending

The cross section near the wall in Figure 2-9 is experiencing inelastic bending. Looking closer at the cross section, the stress and strain profiles are depicted in Figure 2-10.

Figure 2-10 Stress Profile (a) and Strain Profile (b)

The stress profile on the left is clearly non-linear. However, the strain profile does remain linear despite the inelastic stress.

This concept is the basis for the Crotti-Engesser method, which replaces the $\frac{M}{EI}$ term with the variable κ, the inverse of the radius of curvature, to form Equation (2-7). It should be noted that

the Crotti-Engesser approach is appropriate for situations involving non-linear elastic behavior, or plastic behavior that does not include un-loading.

$$\delta_i = \int_o^L \kappa \frac{\partial M_i}{\partial F_i} dx \tag{2-7}$$

One can solve for radius of curvature using the following relation:

$$\varepsilon = \frac{y}{R} \tag{2-8}$$

Where ε is the strain at a point, y is the distance from the neutral axis of bending, and R is the radius of curvature. The value κ, the beam curvature, is the inverse of R.

Utilizing this method can be tricky, if all that is known are the material properties such as a stress strain curve, the loading conditions, and the beam geometry. This is because the moment can be computed, but cannot be related to the stress or strain values resulting at each point in the component using standard equations. Using the strain values given for material properties, the radius of curvature is computed for that strain value, and then the moment for that radius of curvature is computed using Equation (2-9) [11].

$$M_z = \int (\sigma)(dA)(y) \tag{2-9}$$

In the equation above, dA refers to an infinitesimal piece of the cross-sectional area of the beam, y refers to the distance from the neutral axis of bending, and σ refers to the stress in terms of strain. For example, a circular cross section will be considered. Refer to Figure 2-11.

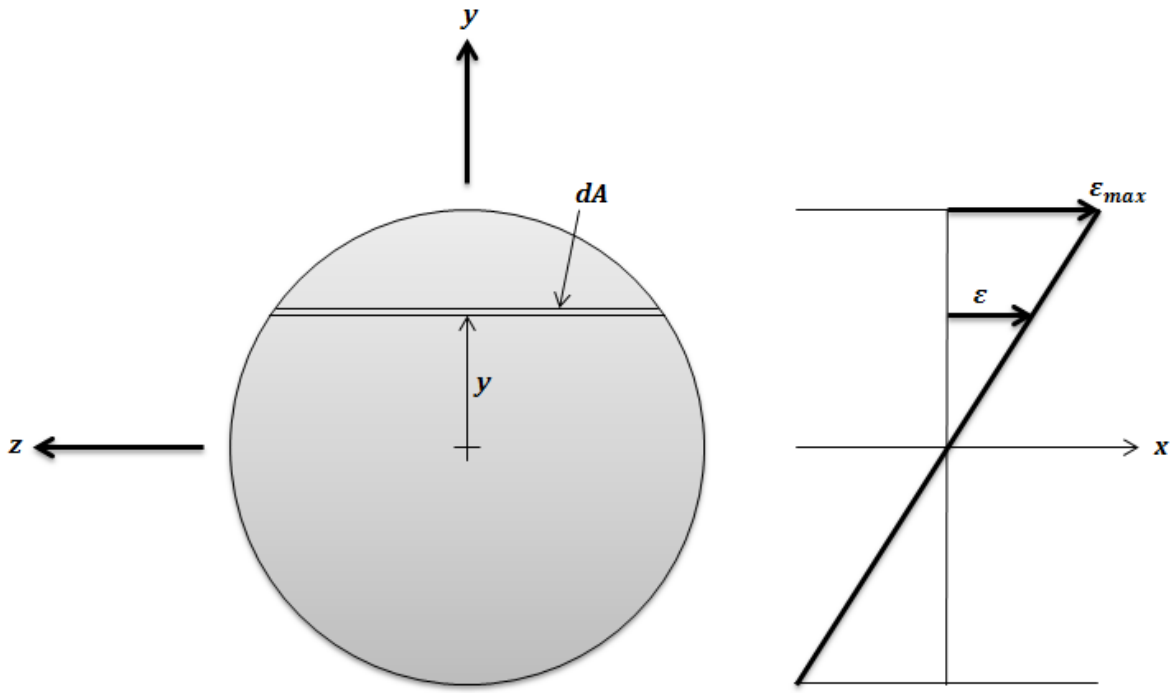

Figure 2-11 Cross Section and Strain Profile

For the cross section above, the equation for the circle must be considered.

$$y^2 + z^2 = \left(\frac{d}{2}\right)^2$$

The first objective would be to determine the *dA* term in Equation (2-9). The equation for the circle is solved for *z* in terms of *y*.

$$z = \left(\left(\frac{d}{2}\right)^2 - y^2\right)^{\frac{1}{2}}$$

Then the infinitesimal area, *dA*, becomes the following expression.

$$dA = 2zdy = 2\left(\left(\frac{d}{2}\right)^2 - y^2\right)^{\frac{1}{2}} dy$$

Next, the stress term, σ, must be written in terms of strain. This can be done if the material properties are known and a stress-strain curve can be developed such as the one shown in Figure 2-12.

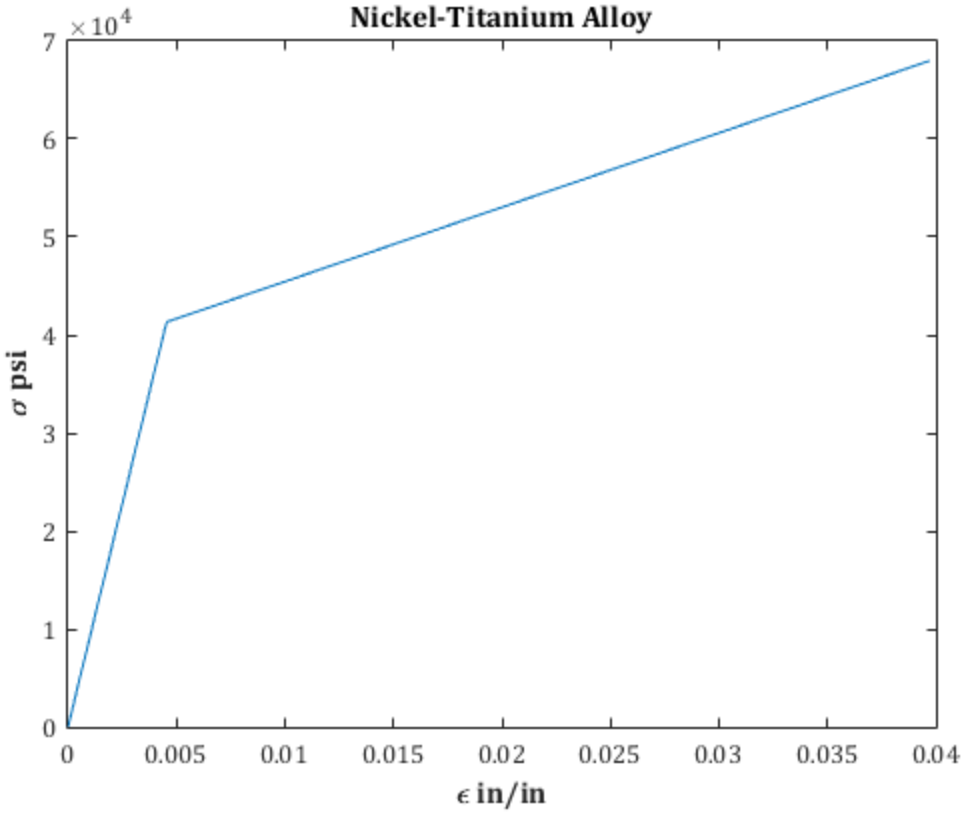

Figure 2-12 Bilinear Stress-Strain Curve

Using the material behavior from Figure 2-12, the stress, σ, can be written as shown below.

$$\sigma = E\varepsilon\left[1 + \left(\frac{1-C}{C}\right)H(\varepsilon, \varepsilon_{y)}\right] + E\varepsilon_y\left(\frac{C-1}{C}\right)H\left(\varepsilon, \varepsilon_y\right) \tag{2-10}$$

Because the example features a bilinear stress strain curve, C is a constant used to adjust the modulus of elasticity for the second portion of the curve. The relationship below can be used for clarity.

$$E_1 = \frac{1}{C}E_2$$

Additionally, the strain value, ε, can be written in terms of y, the distance from the neutral axis of bending.

$$\varepsilon = \frac{2y\varepsilon_{max}}{d}$$

All other terms in the stress equation are constant across the beam cross section. Every term in Equation (2-9) can be written in terms of y. Equation (2-9) can be written as shown below.

$$M_z = 4\int_0^{\frac{d}{2}} y\left(\left(\frac{d}{2}\right)^2 - y^2\right)^{\frac{1}{2}} E\frac{2y\varepsilon_{max}}{d}\left[1 + \left(\frac{1-C}{C}\right)H(\varepsilon, \varepsilon_{y)}\right] + E\varepsilon_y\left(\frac{C-1}{C}\right)H(\varepsilon, \varepsilon_y)dy$$

This can be numerically integrated and evaluated between the bounds to determine the moment associated with a radius of curvature value obtained using Equation (2-8). From this set of data, a moment-curvature relationship can be established, most often in the form of a plot as shown in Figure 2-13.

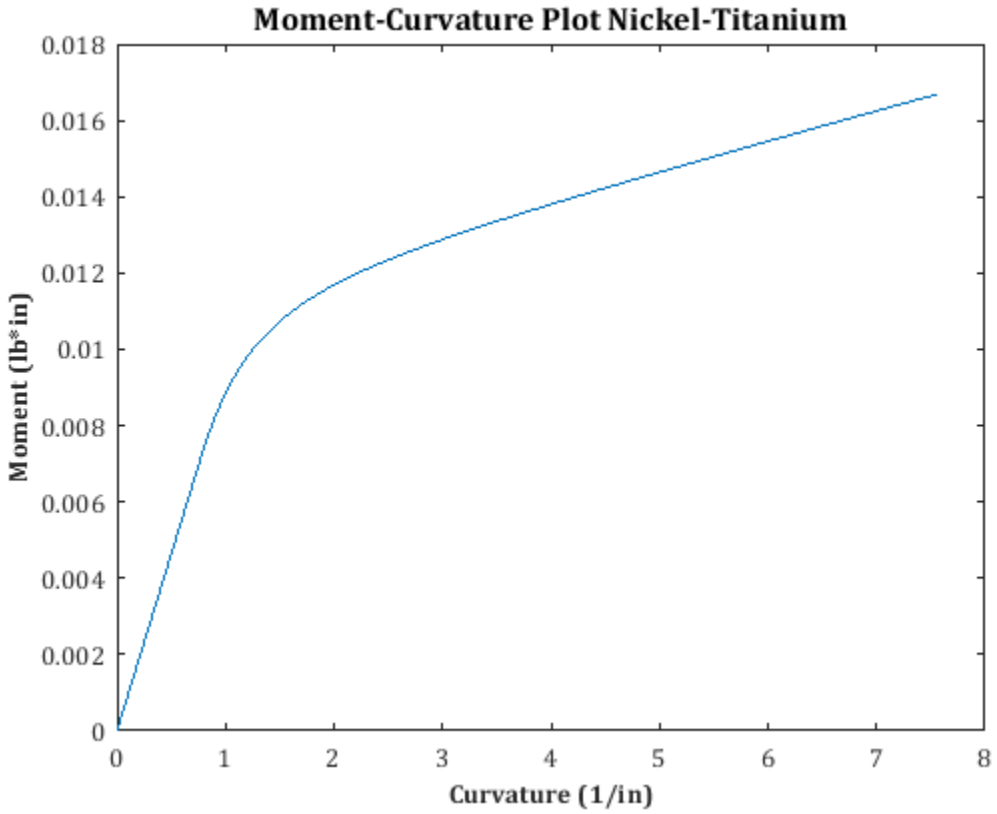

Figure 2-13 Moment-Curvature Plot

Then, the moment along the length of a beam can be computed and curvature values can be determined by interpolating the moment-curvature plot. The radius of curvature values can be used to determine the values for κ in Equation (2-7), and the displacement of the beam can be computed when inelastic bending occurs.

Finite Element Analysis

The way this research was conducted involved three main steps for the base cases as well as the final orthodontic model.

1. Develop a closed-form and numerical solution using the methods previously described in this chapter.
2. Compose a finite element model of the same problem.
3. Compare the results of the closed-form/numerical solution with the results of the finite element analysis.

Finite Element Models

The finite element models used were all created in the 2016 or 2017 student version of Abaqus. All were 2D, deformable wire models. They featured beam sections and elements only. The steps of FEA models were general static, as the loads and displacements were applied over a long period of time. The beam section orientation was established for all models with tangent vectors acting in the axial direction and direction vectors n1 and n2 defined along the cross-sectional plane. An example is shown in Figure 2-14, where vector **t** shown in red is the tangent vector. The beam elements for all models were selected from the standard library and featured a cubic formulation (Euler-Bernoulli) type element with 2 nodes per element. The Abaqus standard library name of the element is B23. Because Euler-Bernoulli type elements were used, transverse shear deformation is not included. Plane sections initially normal to the beam's axis remain plane. This type of element is good for slender beams and suited these models due to the Eulerian Beam theory that was utilized to develop the closed-form solutions.

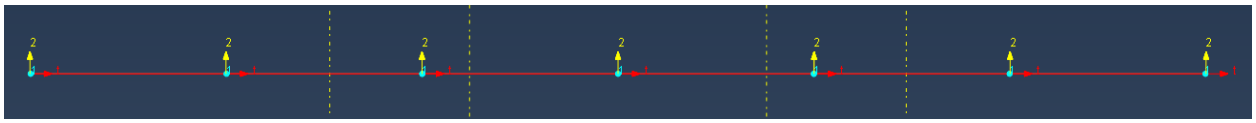

Figure 2-14 Beam Orientation Abaqus

Material Properties

The material used for most of the base cases and one of the final orthodontic models was a nickel-titanium alloy featuring a stress-strain relationship that is best estimated as a bilinear model. The stress-strain behavior is depicted in the graph of Figure 2-12. The value of E_1, or the elastic modulus for the elastic regime, is 9,100,000 psi, and E_2 is approximately $\frac{1}{12}$ the value of E_1. The value of σ_y is approximately 41,300 psi and the value of ε_y is .00454. Material

data was pulled from *Comparison of NiTi Orthodontic Archwires and a Determination of the Characteristic Properties*. [12]

When applying the material properties in Abaqus, only the elastic modulus, E_1 was needed for the elastic behavior. For the plastic behavior, a set of data including yield stresses and the corresponding values for plastic strain was needed.

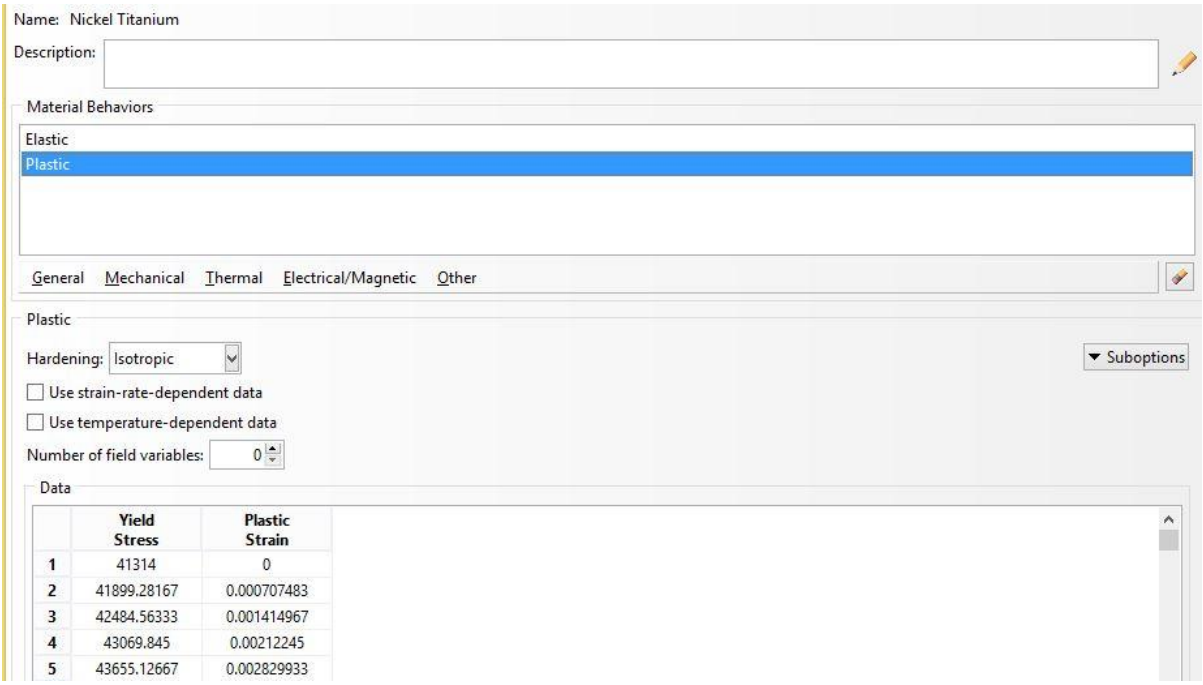

Figure 2-15 Plasticity Model Abaqus

The data was provided by extracting stress and corresponding strain values from Equation (2-10). Using the stress-strain values for the inelastic regime, or the values for which E_2 applies, the elastic portion of the strain was subtracted out, leaving yield stress values and the corresponding values for plastic strain which were used to populate the table shown in Figure 2-15.

A few of the base cases and the elastic final orthodontic model featured a material of stainless steel. The other base cases featured aluminum with an elastic modulus of 1E7 psi and the final orthodontic model that featured 316 stainless steel had an elastic modulus of 2.8E7 psi.

Summary

This chapter introduced the analytical methods of this research as well as the approach taken toward the finite element analysis. The following chapters will introduce multiple simple base cases developed to validate the accuracy of both the analytical methods and the finite

element models. Simple base cases were developed first, and accuracy of the methods established early such that when a more complex final model was created, trouble-shooting would be reduced should a discrepancy arise.

Chapter 3: Closed-form Solutions

Introduction

This chapter introduces simple cases of linear elastic bending in straight beams. The problems presented here have published closed-form solutions. They are presented as validation that the finite element models are accurate and verification of the modified form of Castigliano's theorem.

Case 1

Case 1 was a straight beam of rectangular cross section and a length of 5 inches. The base, *b*, was .057 inches and the height, *h*, of the beam was 0.113 inches. Refer to the cross section in Figure 3-1. The cross-sectional dimensions were chosen to represent realistic geometry of an orthodontic arch wire. The right end of the beam was clamped and a point load, *P*, was applied to the left end. The magnitude of the point load was 1 lb. The beam experienced only elastic bending. The diagram of case 1 is shown in Figure 3-1.

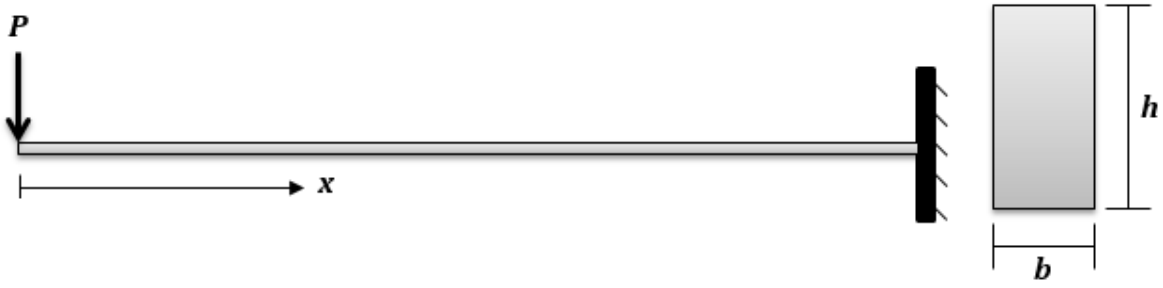

Figure 3-1 Case 1

Analytical Methods

The analytical solution was developed using Castigliano's theorem. Moving toward the fixed end, the moment equation becomes:

$$M(x) = -Px$$

The partial derivative of the moment equation with respect to load *P* is shown below.

$$\frac{\partial M}{\partial P} = -x$$

Now, using the moment and its partial derivative to evaluate Equation (2-2), the integral becomes:

$$\delta_P = \int_o^L \frac{Px^2}{EI} dx,$$

The equation is solved and shown below.

$$\delta_P = \frac{PL^3}{3EI}$$

This is the closed-form solution for the deflection at the end of the beam. In order to solve for the deflection along the length of the beam, a dummy load, Q must be introduced. Q is a fictitious or imaginary load that must be applied at the point where the deflection is to be determined. This is because by definition, Castigliano's Theorem relates a force to a deflection at the point of load application. Q is later set to its true value of zero. When using the dummy load, Q, to solve for deflection along the length of the beam, the scenario becomes:

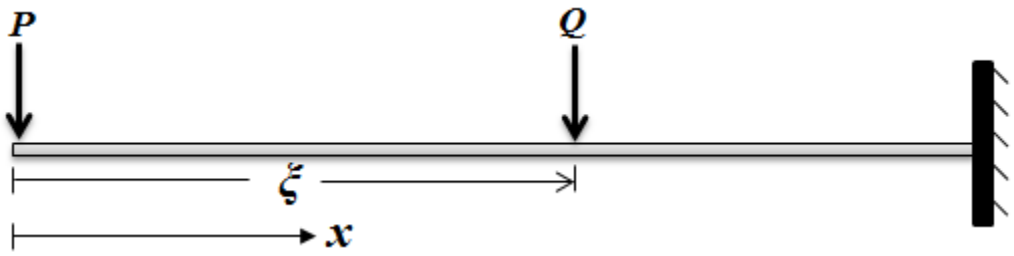

Figure 3-2 Case 1 featuring fictitious load Q

The moment equation becomes:

$$M(x) = -Px - Q(x - \xi) * H(x, \xi).$$

The partial derivative of the moment is taken with respect to Q.

$$\frac{\partial M}{\partial Q} = -(x - \xi) * H(x, \xi)$$

Using the moment equation and its partial derivative in Equation (2-2), the integral becomes:

$$\delta_Q = \int_o^L \frac{-Px - Q(x - \xi) * H(x, \xi)}{EI} * -(x - \xi) * H(x, \xi)\, dx$$

The Heaviside step function present in the integral will evaluate to zero when $x<\xi$. In this case, the bounds of integration can be changed, the Heaviside step function evaluated to one, and therefore dropped. The value of Q is set to its true value of zero and the integral becomes:

$$\delta_Q = \int_{\xi}^{L} \frac{-Px}{EI} * -(x-\xi)\, dx$$

The integral is solved and the equation becomes:

$$\delta_Q = \frac{Px^3}{3EI} - \frac{Px^2\xi}{2EI}\Bigg|_{\xi}^{L}$$

After evaluation using the upper and lower bounds, the deflection at any location along the beam can be determined. Below is the closed-form solution for deflection along the length of the beam.

$$\delta_Q = \frac{P}{6EI}(2L^3 - 3L^2\xi + \xi^3)$$

After formulating the closed-form solution, the focus was shifted to developing the finite element model. The finite element model was created in Abaqus. The boundary conditions and loading are shown in Figure 3-3. The right end was fixed from translation and rotation about all 3 axes, in order to produce the cantilevered end condition. The load was introduced as a point load at the left end of the beam, as shown below. The cross section created for the model used the same dimensions presented in Figure 3-1. The model featured 981 nodes and 980 elements.

Figure 3-3 Case 1 Abaqus

The vertical displacement was simulated for the length of the beam.

Aside from the closed-form solution and the finite element model, a numerical solution was developed. The numerical solution was created in TK solver by Dr. Edwin Odom. It employed the same methods described in the *analytical methods* section, but utilized numerical integration instead of symbolic integration as shown above.

A comparison was made between the FEA results the results obtained both numerically and analytically. The comparison between the three is presented in the results section below. Refer to Figure 3-8.

Results

Figure 3-4 shows the vertical displacement from the finite element analysis. Note that the *y*-direction is denoted U2 and the units are inches. The deflection is scaled 1:1 for viewing purposes.

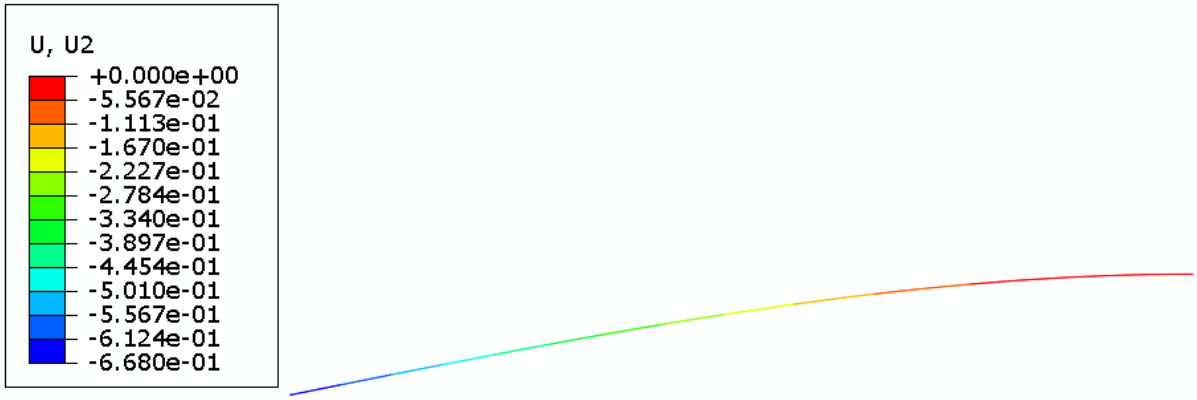

Figure 3-4 Case 1 Abaqus Vertical Displacement

The deflection along the length of the beam was compared between the FEA model, the analytical solution, and the numerical solution. The results comparing the FEA and analytical solution are plotted below in Figure 3-5. The difference is miniscule and cannot be distinguished when plotted using standard methods.

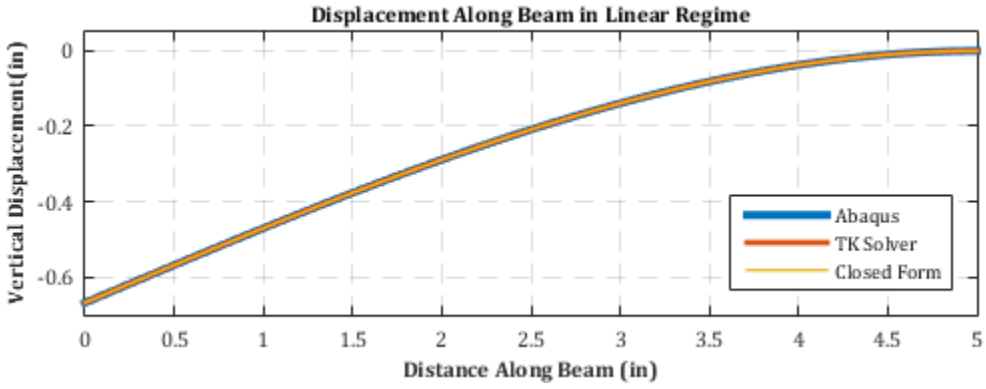

Figure 3-5 Case 1 Vertical Displacement of Cantilevered Beam

Case 2

Case 2 was a simply supported beam with a point load applied mid-span. The setup is shown in Figure 3-6 and the free body diagram is shown in Figure 3-7.

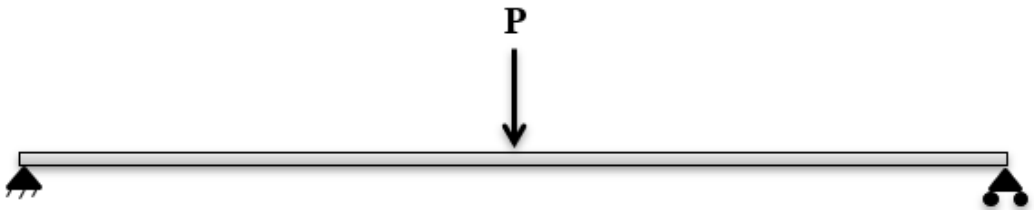

Figure 3-6 Case 2

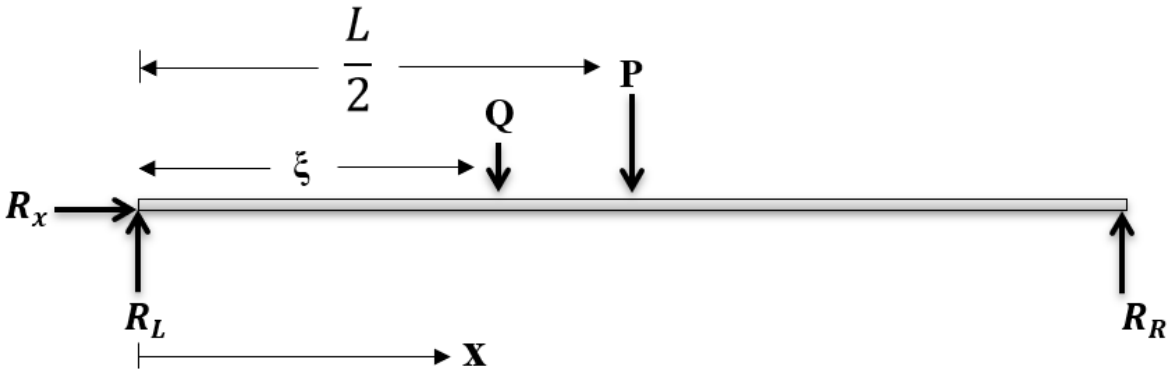

Figure 3-7 Case 2 Free Body Diagram

Analytical Methods

It can be seen that the value of R_x is zero, as it is the only force in the x-direction caused by the pinned connection at the left end. Note again that Q arises as a fictitious load with a value of zero. It is introduced so the deflection at each point where Q is applied can be determined. This way the deflection along the entire length of the beam can be determined.

The problem solution begins by taking the moment equation.

$$M(x) = R_L x - Q(x-\xi) * H(x,\xi) - P\left(x - \frac{L}{2}\right) * H(x,\frac{L}{2})$$

Because this beam does not have a completely fixed end condition, Lagrange multipliers will be involved. Refer to chapter two for the reasoning and theory behind this.

The sum of the forces in the y-direction is taken. This equation is denoted as g_1.

$$g_1 = \sum y = 0 = R_L - P - Q + R_R$$

And the sum of the moments, denoted g_2 is taken about the right end of the beam.

$$g_2 = \sum M_R = 0 = R_L L - Q(L - \xi) - \frac{PL}{2}$$

It can be seen by looking at g_1 and the moment equation, $M(x)$, that R_R does not occur in the moment equation, therefore R_R is implicit. Additionally, R_R is non-working because the displacement caused by R_R is zero. Because the force R_R appearing in g_1 is implicit and non-working, g_1 can be ignored. There will not be a Lagrange multiplier associated with g_1.

By examining g_2 it can be seen that all the forces that appear in g_2 also appear in the moment equation. Therefore, g_2 cannot be ignored and there will be a Lagrange multiplier, λ_2, associated with g_2.

The value for this Lagrange multiplier, λ_2, must be determined in order to solve the rest of the problem and determine the deflection along the length of the beam. The displacement equation for the left end of the beam will be utilized to solve for λ_2, since the deflection at the left end is known to be zero. The following form of Equation (2-3) will be used:

$$\delta_L = \int_0^L \frac{M_{Q=0}}{EI} \frac{\partial M}{\partial R_L} dx + \lambda_2 \frac{\partial g_2}{\partial R_L}$$

The two partial derivatives are computed as follows.

$$\frac{\partial M}{\partial R_L} = x$$

$$\frac{\partial g_2}{\partial R_L} = L$$

The partial derivatives and the moment equation will be used to evaluate the integral. Note that the value of Q is zero. The terms including Q are dropped in the integral to account for the fact that Q is a fictitious load. Additionally, the value of δ_L is known to be zero. The equation becomes:

$$0 = \int_0^L \frac{R_L x - P\left(x - \frac{L}{2}\right) * H(x, \frac{L}{2})}{EI} * x dx + \lambda_2 L$$

For values of x less than $\frac{L}{2}$, the term including the force P is zero since the Heaviside step function is zero in this region. Therefore, the integral only includes the value with P for values

of x between L and $\frac{L}{2}$, and the equation above can be broken down into parts to take the following form.

$$0 = \int_0^L R_L x^2 dx - \int_{\frac{L}{2}}^L Px(x - \frac{L}{2})dx + \lambda_2 LEI$$

After evaluating both integrals, the equation becomes:

$$0 = \frac{R_L L^3}{3} - \frac{5PL^3}{48} + \lambda_2 LEI$$

From equation g_1, it is seen that R_L can be replaced with $\frac{P}{2}$. After combining like terms, the equation simplifies significantly as shown below.

$$0 = \frac{PL^3}{6} - \frac{5PL^3}{48} + \lambda_2 LEI$$

This equation is important because the Lagrange multiplier, λ_2 can be solved for in terms of P. Using the equation above, the Lagrange multiplier is determined.

$$\lambda_2 = -\frac{3PL^2}{48EI}$$

Now λ_2 can be used in Equation (2-3) to solve for the deflection at every point Q, along the beam.

$$\delta_Q = \int_0^L \frac{M_{Q=0}}{EI}\frac{\partial M}{\partial Q}dx + \lambda_2 \frac{\partial g_2}{\partial Q}$$

The first partial derivative is:

$$\frac{\partial M}{\partial Q} = -(x - \xi) * H(x, \xi)$$

And the second partial derivative is:

$$\frac{\partial g_2}{\partial Q} = -(L - \xi)$$

Using the partial derivatives and the moment equation with Q set to zero, the equation for displacement becomes:

$$\delta_Q = \int_0^L \frac{R_L x - P\left(x - \frac{L}{2}\right) * H(x, \frac{L}{2})}{EI} * -(x - \xi) * H(x, \xi) dx - \lambda_2 (L - \xi)$$

There are two Heaviside step functions in the integral. To simplify operations, the integral will be broken down into two simpler integrals. For the first integral, there was only one Heaviside step function associated, and the bounds of integration have been adjusted to account for it. However, in the second integral, there are two Heaviside step functions. See the identity below for this situation.

$$EI\delta_Q = \int_\xi^L -R_L x(x - \xi) dx + \int_0^L P\left(x - \frac{L}{2}\right) H\left(x, \frac{L}{2}\right)(x - \xi) H(x, \xi) dx - \lambda_2 EI(L - \xi)$$

The following identity must be used.

$$H\left(x, \frac{L}{2}\right) H(x, \xi) = H\left(x, \frac{L}{2}\right) if\ \frac{L}{2} > \xi. Else\ H\left(x, \frac{L}{2}\right) H(x, \xi) = H(x, \xi)$$

Using this identity, the focus is shifted to just the second integral, which can be re-written:

$$\int_{\frac{L}{2}}^L P\left(x - \frac{L}{2}\right)(x - \xi) dx + H(\xi, \frac{L}{2}) \int_\xi^{\frac{L}{2}} P\left(x - \frac{L}{2}\right)(x - \xi) dx$$

Now that the identity has been utilized, there are more integrals; however, they are simpler and can be evaluated using standard methods. Putting the integrals above back into the entire equation, the displacement is written as shown below.

$$EI\delta_Q = \int_\xi^L -R_L x(x - \xi) dx + \int_{\frac{L}{2}}^L P\left(x - \frac{L}{2}\right)(x - \xi) dx + H\left(\xi, \frac{L}{2}\right) \int_\xi^{\frac{L}{2}} P\left(x - \frac{L}{2}\right)(x - \xi) dx - \lambda_2 EI(L - \xi)$$

After the integrals are evaluated between the specified bounds, the closed-form solution becomes:

$$EI\delta_Q = -\frac{P(L - \xi)^2(2L + \xi)}{12} + \frac{L^2 P(5L - 6\xi)}{48} - H\left(\xi, \frac{L}{2}\right) \frac{P(L - 2\xi)^3}{48} - \lambda_2 EI(L - \xi)$$

The value for λ_2 was determined in the previous steps. It is substituted into the equation above to produce the closed-form solution for the displacement along the length of the beam.

$$\delta_Q = -\frac{P}{12EI}\left((L-\xi)^2(2L+\xi)\right) + \frac{P}{48EI}(L^2(5L-6\xi)) - H\left(\xi,\frac{L}{2}\right)\frac{P}{48EI}((L-2\xi)^3) + \frac{P}{48EI}(3L^2(L-\xi))$$

The equation above is the closed-form solution for the displacement along the length of the beam.

This problem was constructed in Abaqus to validate the analytical results. For the example, the beam was made of aluminum with an elastic modulus of 1E7 psi and a circular cross section with a diameter of .6718 inches. This was such that the *EI* term came out to an even magnitude of 10,000. The length of the beam was 20 inches and a point load of 30 pounds applied at 10 inches from the left end, or mid-span. The boundary conditions and loading are shown below. The left end is fixed in the *x* and *y*-direction, and the right end is fixed in only the *y*-direction. The model included 801 nodes and 800 elements.

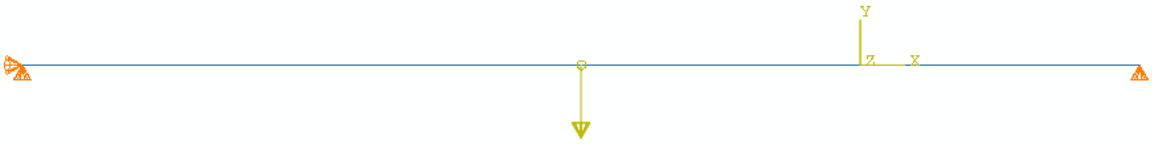

Figure 3-8 Case 2 Abaqus

The vertical displacement of the beam simulated using Abaqus is presented in the following results section. See Figure 3-9. Additionally, a comparison is made between the FEA solution, the closed-form solution derived above, and the numerical solution. The numerical solution employed the same concepts shown in the *analytical methods* section above. However, numerical integration was used in TK solver, instead of symbolic integration. Refer to Figure 3-10.

Results

Figure 3-9 shows the vertical displacement of the beam obtained from the finite element analysis. The color scale on the left hand side gives the displacement in units of inches.

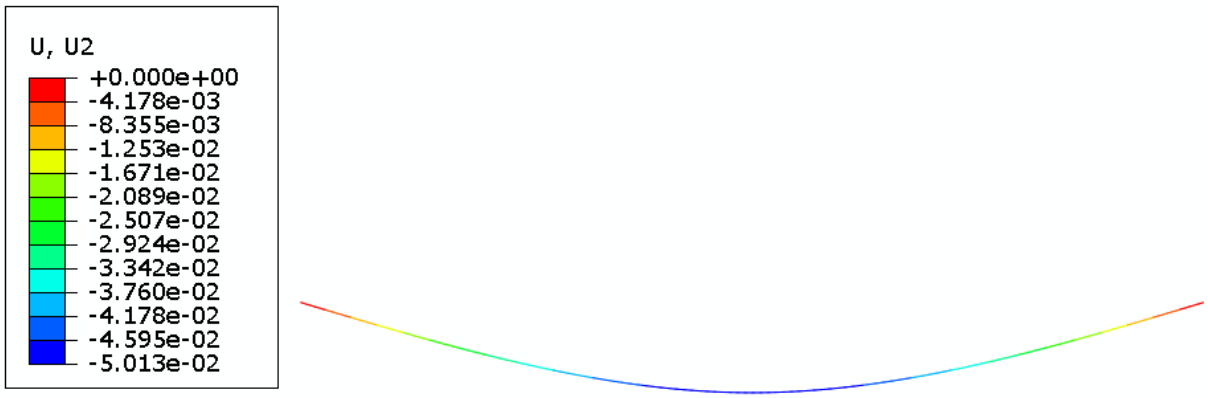

Figure 3-9 Case 2 Abaqus Vertical Displacement

Figure 3-10 shows the vertical displacement of the beam obtained using FEA, numerical integration, and the closed-form solution.

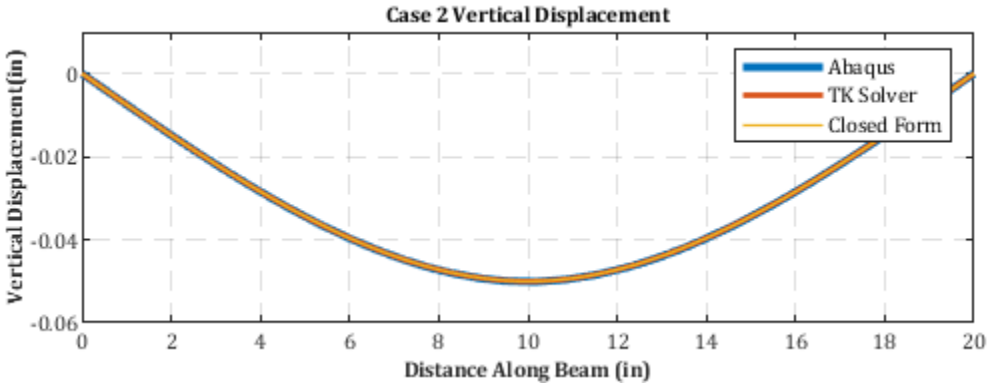

Figure 3-10 Case 2 Vertical Displacement

Discussion

For the cases presented in this chapter, FEA, numerical methods, and the closed-form solution produce almost identical results. This is a good indicator that the modified form of Castigliano's theorem can accurately be applied to non-traditional problems, and that the finite element model is constructed appropriately and accurately. The FEA can be trusted to validate more complicated problems when a closed-form solution may not exist or be available.

Chapter 4: Statically Indeterminate Beams

Introduction

After the success demonstrated with cantilevered and simply supported beams subjected to elastic bending in the previous chapter, the studies progressed to applying the mathematical methods to a statically indeterminate beam problem. The closed-form solution and the finite element solution are presented below.

Case 3

First, the statically indeterminate problem will be introduced in Figure 4-1 below. This problem is from the class notes of one of Professor Jus' students.

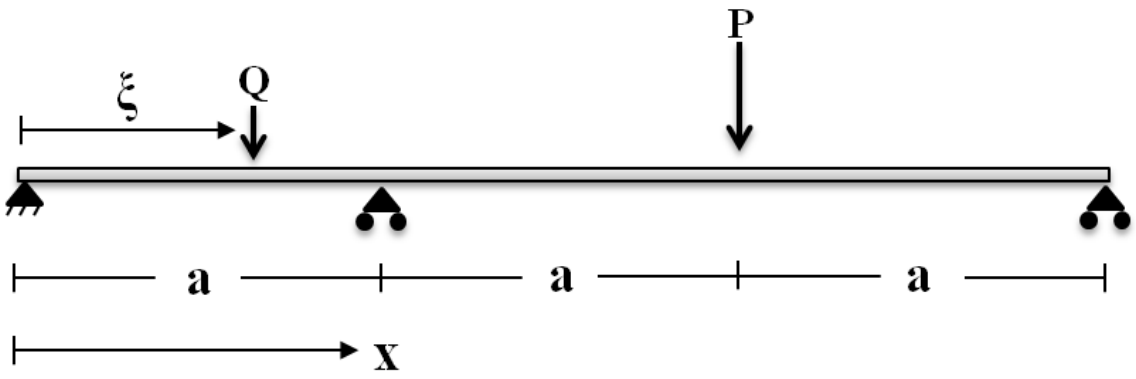

Figure 4-1 Case 3

The beam featured a pinned connection at the left end, a roller support one third of the length from the left end, a point load two thirds length from the left end, and a roller support at the right end. The free body diagram is shown in Figure 4-2.

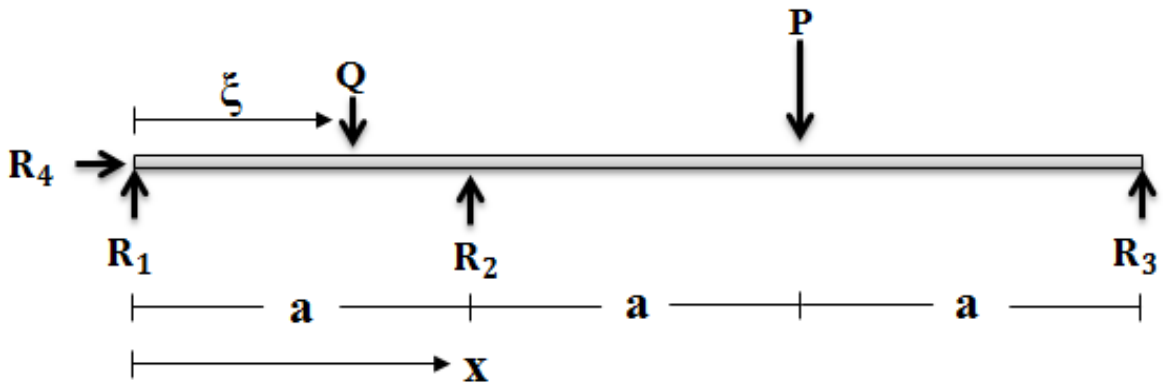

Figure 4-2 Case 3 Free Body Diagram

Analytical Methods

First, it should be noted that R_4 arises from the pinned connection at the left end. Because this is the only force in the x-direction, its value is zero. Additionally, the load Q is a fictitious load with a true value of zero which is used to calculate the displacement at a point of interest located at a distance ξ from the left end of the beam. Starting from the left end, the moment equation is constructed below.

$$M(x) = R_1 x - Q(x-\xi) * H(x,\xi) + R_2(x-a) * H(x,a) - P(x-2a) * H(x,2a)$$

The equations of equilibrium are needed in order to determine the Lagrange multipliers. First, the sum of the forces is taken in the y-direction and denoted g_1.

$$g_1 = \sum Fy = 0 = R1 + R2 + R3 - P - Q \tag{1}$$

Next, the sum of the moments is taken about the right end of the beam and denoted as g_2.

$$g_2 = \sum M_R = 0 = R_1 L - Q(L-\xi) + R_2(2a) - Pa \tag{2}$$

Looking at g_1, the R_3 term does not appear in the moment equation, making it implicit. Additionally, the displacement at R_3 is zero, and it is therefore non-working. Because a force present in g_1 is implicit and non-working, g_1 can be ignored. Now, looking at g_2, it can be seen that all the force terms: R_1, R_2, Q, and P also appear in the moment equation, making them explicit. This means that g_2 cannot be ignored and there will be a Lagrange multiplier associated with it.

Next, the displacement at the left end of the beam is known to be zero. The following form of Equation (2-3) can be used.

$$0 = \int_o^L \frac{M_{Q=0}}{EI}\frac{\partial M}{\partial R_1}dx + \lambda_2 \frac{\partial g_2}{\partial R_1}$$

First, the partial derivatives featured in the equation above must be determined.

$$\frac{\partial M}{\partial R_1} = x$$

$$\frac{\partial g_2}{\partial R_1} = L$$

Next, the moment equation, with Q set to its true value of zero, and the two partial derivatives above can be implemented.

$$0 = \int_0^L \frac{R_1 x + R_2(x-a)H(x,a) - P(x-2a)H(x,2a)}{EI} * x + \lambda_2 L$$

This can be broken down as shown below to make evaluation of the integrals simpler.

$$0 = R_1\int_0^L x^2 dx + R_2\int_a^L x(x-a)dx - P\int_{2a}^L x(x-2a)dx + \lambda_2 LEI$$

The Heaviside step functions are no longer included, as the bounds of integration have been adjusted to account for only the cases where the function evaluates to one, as opposed to zero. Additionally, the forces are constant and have been pulled outside the integral for simplification. After evaluating the integrals, the equation becomes:

$$0 = \frac{R_1 L^3}{3} + R_2\left[\frac{L}{2}(L-a)^2 - \frac{(L-a)^3}{6}\right] - P\left[\frac{L}{2}(L-2a)^2 - \frac{(L-2a)^3}{6}\right] + \lambda_2 LEI$$

Since a=$\frac{L}{3}$, the equation can be simplified:

$$0 = \frac{R_1 L^3}{3} + \frac{14R_2 L^3}{81} - \frac{4PL^3}{81} + \lambda_2 LEI$$

By dividing out the $\frac{L^3}{3}$ term, once more the equation can be further simplified.

$$0 = R_1 + \frac{14}{27}R_2 - \frac{4}{27}P + \frac{3\lambda_2 EI}{L^2} \tag{3}$$

Additionally, the vertical displacement at the location of R_2 is zero. This zero-displacement condition must be used to create a second equation to assist in reaching the goal of determining values for R_1, R_2, R_3 and λ_2. First, the partial derivatives of the moment and g_2 must be taken with respect to R_2.

$$\frac{\partial M}{\partial R_2} = (x - a) * H(x, a)$$

$$\frac{\partial g_2}{\partial R_2} = 2a$$

These partial derivatives will be used in Equation (2-3) shown below.

$$0 = \int_o^L \frac{M_{Q=0}}{EI}\frac{\partial M}{\partial R_2}dx + \lambda_2 \frac{\partial g_2}{\partial R_2}$$

Using the partial derivatives and the moment equation with Q set to its true value of zero, the equation becomes:

$$0 = \int_0^L \frac{R_1 x + R_2(x-a)H(x,a) - P(x-2a)H(x,2a)}{EI} * (x-a)H(x,a)dx + \lambda_2 2a$$

This integral can be broken up into segments, and the bounds of integration adjusted to account for the cases where the Heaviside step functions are one, and eliminating the cases where they cause the integral to evaluate to zero.

$$0 = R_1 \int_a^L x(x-a)dx + R_2 \int_a^L (x-a)^2 dx - P\int_{2a}^L (x-a)(x-2a)dx + \lambda_2 2aEI$$

After evaluating the integrals, the equation is now:

$$0 = \frac{14R_1L^3}{81} + \frac{R_2}{3}(L-a)^3 - \frac{P}{2}\left[(L-a)(L-2a)^2 - \frac{(L-2a)^3}{6}\right] + \lambda_2 2aEI$$

This equation can be further simplified by substituting a=$\frac{L}{3}$.

$$0 = \frac{14R_1L^3}{81} + \frac{8R_2L^3}{81} - \frac{5PL^3}{162} + \frac{2}{3}\lambda_2 LEI$$

This equation further reduces to:

$$0 = R_1 + \frac{4R_2}{7} - \frac{5}{28}P + \frac{27\lambda_2 EI}{7L^2} \tag{4}$$

Now, there are four equations and four unknowns. After solving the system of equations, the values for the three reaction forces and the value for λ_2 were determined.

$$R_1 = -\frac{1}{4}P$$

$$R_2 = \frac{7}{8}P$$

$$R_3 = \frac{3}{8}P$$

$$\lambda_2 = -\frac{PL^3}{54EI}$$

With these four variables, the equation for displacement along the length of the beam is constructed.

$$\delta_Q = \int_0^L \frac{M_{Q=0}}{EI}\frac{\partial M}{\partial Q}dx + \lambda_2 \frac{\partial g_2}{\partial Q}$$

Using the moment equation with Q set to zero and the partial derivatives with respect to the fictitious load Q at the point of interest, the equation becomes:

$$\delta_Q = \int_0^L \frac{R_1 x + R_2(x-a)H(x,a) - P(x-2a)H(x,2a)}{EI} * -(x-\xi)H(x,\xi)dx - \lambda(L-\xi)$$

Breaking this up into simpler integrals, and adjusting the bounds of integration to account for the Heaviside step functions, the equation becomes:

$$\delta_Q = -\frac{R_1}{EI}\int_\xi^L x(x-\xi)dx - \frac{R_2}{EI}\left[\int_a^L -H(\xi-a)\int_a^\xi (x-a)(x-\xi)dx\right] + \frac{P}{EI}\left[\int_{2a}^L -H(\xi-2a)\int_{2a}^\xi (x-2a)(x-\xi)dx\right] + \frac{PL^2(L-\xi)}{54EI}$$

After evaluating the integrals, the equation takes the form below.

$$\delta_Q = \frac{1}{EI}\left\{-\frac{R_1}{2}\left[L(L-\xi)^2 - \frac{(L-\xi)^3}{3}\right] - \frac{R_2}{2}\left[(L-\xi)(L-a)^2 - \frac{(L-a)^3}{3}\right] + \frac{R_2}{3}H(x,0)\left[-\frac{(\xi-a)^3}{3}\right] + \frac{P}{2}\left[(L-\xi)(l-2a)^2 - \frac{(L-2a)^3}{3} + \frac{(\xi-2a)^3}{3}H(x,2a)\right]\right\} + \frac{PL^2(L-\xi)}{54EI}$$

Because all the values for the forces and the value for λ_2 were solved for previously, they can be used to simplify the equation.

$$EI\delta_Q = P\left[\frac{\xi}{216}(9\xi^2 - L^2) - \frac{7}{48}\left(\xi - \frac{L}{3}\right)^3 H(x,a) + \frac{1}{6}\left(\xi - \frac{2L}{3}\right)^3 H(x,2a)\right]$$

The equation above is the closed-form solution for the deflection along the length of the beam where a load Q is applied at a distance ξ from the left end of the beam.

A finite element model of this case was constructed in Abaqus. For the example, the value of P was 30 pounds, the value of a was 10 inches, the elastic modulus, E, was 10^7 psi, and the moment of inertia, I, was .01 in^4. The left end of the beam was fixed in the x and y-direction. The point where R_2 is applied and the right end of the beam are constrained in the y-direction. The loading and constraints are shown in Figure 4-3. The model included 301 nodes and 300 elements.

Figure 4-3 Case 3 Abaqus

The results of the finite element analysis are presented at the end of this chapter. Refer to Figure 4-4.

Additionally, a numerical solution to this same problem was developed by Dr. Edwin Odom. The numerical solution was programmed in TK Solver. It utilized the mathematical concepts presented in the closed-form solution above, which was developed by Dr. Frederick D. Ju. The vertical displacement values from the TK code, and the vertical displacement values from the

FEA were plotted and compared to the closed-form solution. The results are presented in the following section. See Figure 4-5.

Results

The results from the finite element analysis are shown in the figure below. The color scale shows the vertical displacement in units of inches. The displacement has been visually magnified 100x for viewing purposes.

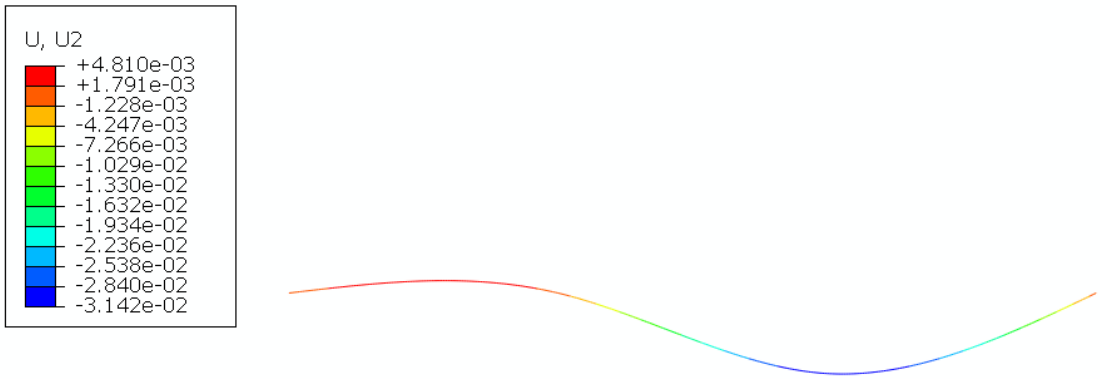

Figure 4-4 Case 3 Abaqus Vertical Displacement

The vertical displacement is compared for the numerical, FEA, and closed-form solutions. The results can be seen in Figure 4-5.

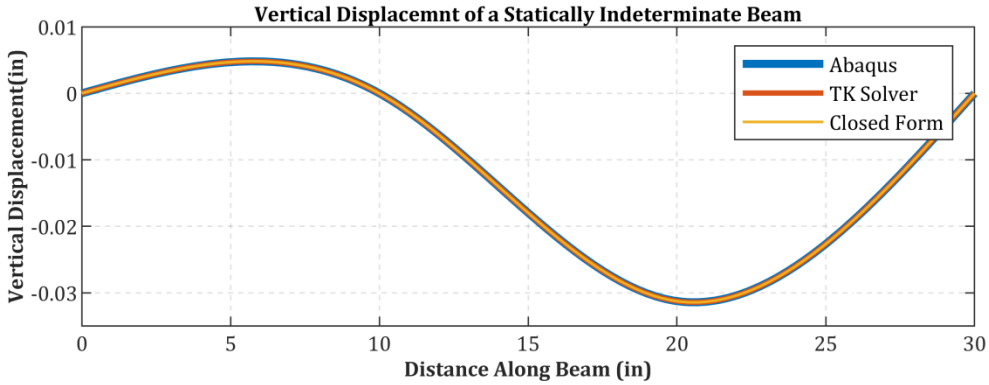

Figure 4-5 Case 3 Vertical Displacement

Discussion

The error between the solutions cannot be perceived using standard graphing methods. Because the modified version of Castigliano's theorem including the use of the Lagrange multiplier, λ_2, was utilized to develop the numerical solution, the fact that the displacement values from both sources match so closely is a good indicator that the modified theorem is accurate, and that the finite element model was constructed correctly.

Chapter 5: Beams and Inelastic Bending

Introduction

This chapter introduces a problem involving inelastic bending. Different formulas and methods must be used to solve these problems. A closed-form solution will not be presented due to their complexity. This chapter will only feature a background on the mathematic principles utilized, and then make a comparison between the FEA model and numerical model only.

Case 4

Case 4 featured a cantilevered beam with a single point load applied at the left end, as shown in Case 1. See Figure 5-1 below.

Figure 5-1 Case 4

However, for Case 4, the load, *P*, was increased such that the beam exceeded its yield point and experienced inelastic bending.

Analytical Methods

As discussed in chapter two, Eulerian beam behavior was assumed for the problems presented in this thesis. As the beam experiences inelastic bending, the stress profile becomes non-linear, but the strain profile remains linear. Refer to Figure 2-6. The original form of Castigliano's theorem represented in Equation (2-2) cannot be applied.

The strain values must be used to determine the radius of curvature, *R*, shown in Equation (2-8). Recall that *y* is the distance from the neutral axis of bending. Equation (2-8) is presented again for easy reference.

$$\varepsilon = \frac{y}{R}$$

Once R is determined, it can be used to determine its inverse, κ, which can be used to replace the $\frac{M}{EI}$ term in the equation for Castigliano's theorem. The variable κ is commonly referred to as the beam curvature. Values of curvature can be obtained through interpolation of data presented in a moment-curvature plot such as the one presented in Figure 2-13. The equation will then take the form of Equation (2-7), introduced again for convenience.

$$\delta_i = \int_o^L \kappa \frac{\partial M_i}{\partial F_i} dx$$

This equation can be used to solve for the deflection of a beam even if it experiences inelastic bending. This approach is referred to as the Crotti-Engesser method.

The finite element model was created in Abaqus. It began with the same model used for Case 1. However, the material data includes inelastic behavior, and the load, P, was increased to 1.5 pounds. This caused inelastic bending to occur near the wall. As shown in Figure 5-2, the right end was fixed from translation and rotation about all 3 axes. The load was introduced as a point load at the left end of the beam, as shown below. The cross section created for the model used the same dimensions presented in Figure 3-1. Refer back to the figure if needed. The model featured 981 nodes and 980 elements.

Figure 5-2 Case 4 Abaqus

The vertical displacement was calculated for the length of the beam. The results for are presented in the results section below. Case 4 was also solved using numerical integration in TK Solver. The comparison between the numerical solution and the finite element model are presented in the results section. Refer to Figure 5-4.

Results

The results of the finite element analysis are presented in Figure 5-3. It shows the vertical displacement of the beam when subjected to the 1.5-pound load. The color scale on the left-hand side has units of inches. The displacement is scaled 1:1 for visual purposes.

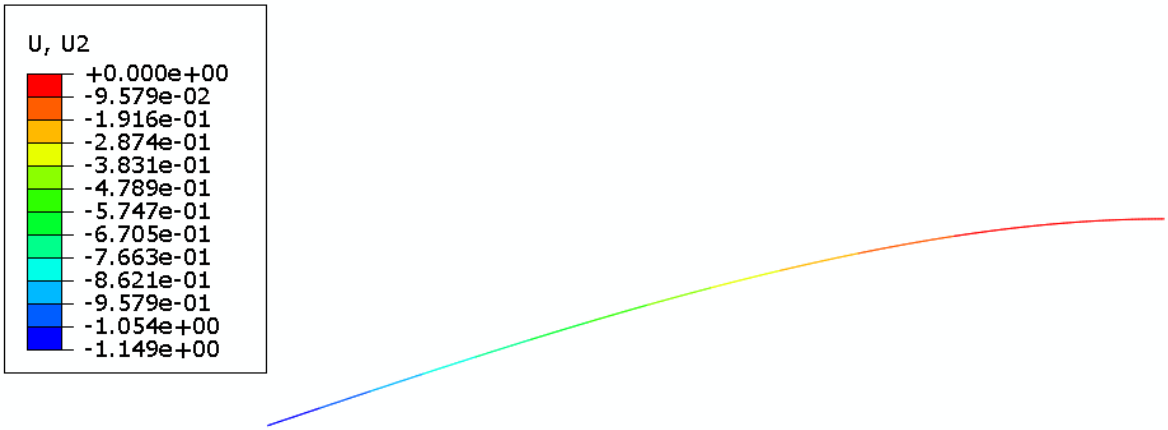

Figure 5-3 Case 4 Abaqus Vertical Displacement

Below is a comparison of the results of obtained using finite element analysis and numerical integration using TK Solver. The graphs are very close.

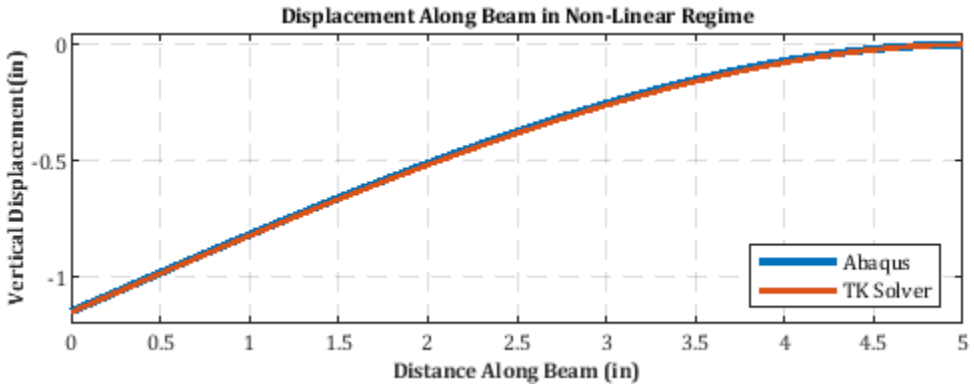

Figure 5-4 Case 4 Vertical Displacement

Discussion

The numerical model featured the same methods which would be used to develop a closed-form solution to this problem, apart from numerical integration. The closeness of the two solutions implies the finite element model created for non-linearity is accurate and can be applied to a more complex problem involving non-linear behavior.

Chapter 6: Curved Beams

Introduction

Until this point, the base cases featured only straight beams. The set of base cases introduced in this chapter are of a semi-circular geometry.

Case 5

Case 5 was a curved beam featuring a rectangular cross section with a width, *b*, of .0562 inches and a height, *h*, of .113 inches. The radius of the beam, *R*, was 5 inches. A point load of 1 pound was applied to the right end in the *x*-direction. The left end was completely fixed. Refer to Figures 6-1 and 6-2. The entire closed-form solution to these problems will not be derived due to its complexity. The chapter will conclude with a comparison between a finite element models and the numerically integrated models.

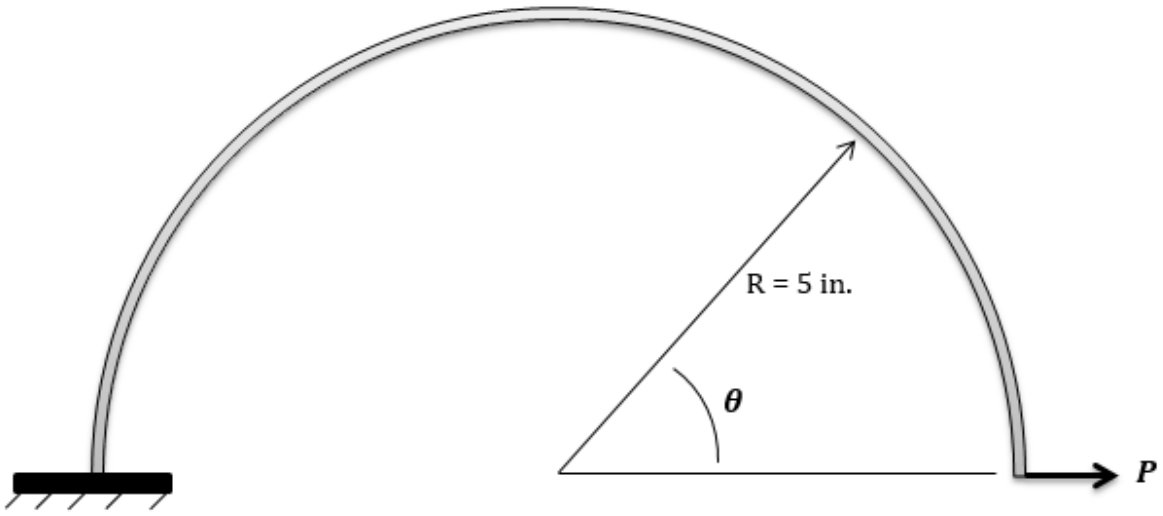

Figure 6-1 Case 5

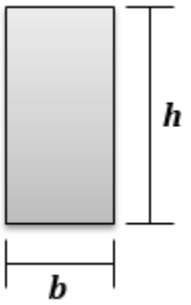

Figure 6-2 Case 5 Beam Cross-Section

Analytical Methods

The moment equation for this problem is shown below.

$$M = P * Rsin\theta$$

The partial derivative of the moment equation with respect to the force *P* is:

$$\frac{\partial M}{\partial P} = Rsin\theta$$

The moment equation and its partial derivative can be used in Equation (2-2) to produce the following result.

$$\delta_P = \frac{1}{EI}\int_o^\pi PRsin\theta * Rsin\theta * R\, d\theta$$

Note that the 3rd case of *R* appears inside the integral next to $d\theta$. This is to change an infinitesimal angle $d\theta$ into an infinitesimal arc length $Rd\theta$, which is integrated over the length of the curved beam. The integral can be simplified to:

$$\delta_P = \frac{1}{EI}\int_o^\pi PR^3 sin^2\theta\, d\theta$$

After evaluating the integral with respecct to θ between the bounds of integration, the equation for δ_P becomes:

$$\delta_P = \frac{\pi PR^3}{2EI}$$

Using this equation, the deflection in the direction of the load *P* was calculated at the end of the beam where *P* is applied. The deflection over the entire range of θ would involve a fictitious load Q.

The finite element model was created in Abaqus. The curved beam with 5" radius was constructed and constrained as shown in Figure 6-3. Rotation and translation about all three axes was restricted on the left end of the beam. The cross-sectional dimensions matched those of Figure 6-2. The load, *P*, of 1 lb was applied at the right end as shown. The model included 787 nodes and 786 elements. The material used for the curved beam models was the nickel-titanium alloy featuring an elastic modulus of 9.1E6 psi.

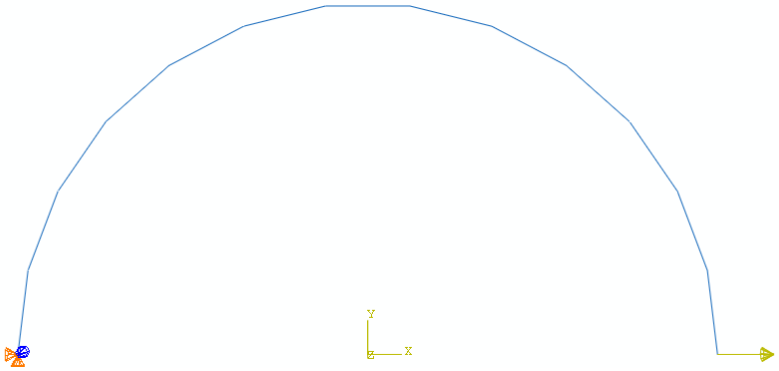

Figure 6-3 Case 5 Abaqus

The results of the finite element analysis are presented in the results section of this chapter. Dr. Odom also developed a numerical model in TK Solver. The comparisons between the two solutions are presented in the results section.

Results

Figure 6-4 shows the results of the finite element anslysis for case 5. The color scale on the left hand side gives the values for the horizontal deflection in inches. The deformation of the beam model is scaled 1:1 for viewing purposes.

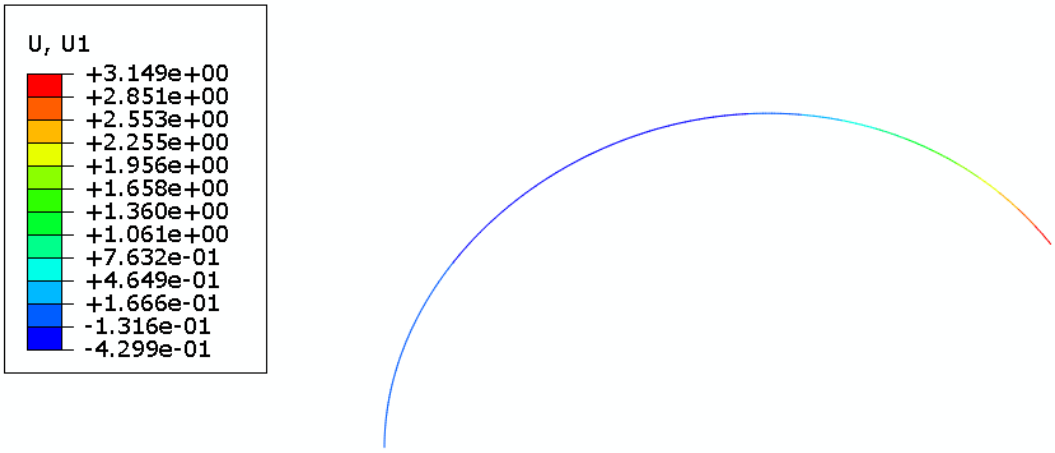

Figure 6-4 Case 5 Abaqus Horizontal Displacement

Below is a graph comparing displacements obtained numerically using TK Solver and by finite element analysis. The graph is a plot of the deformed coordinates of each analyzed point along the beam.

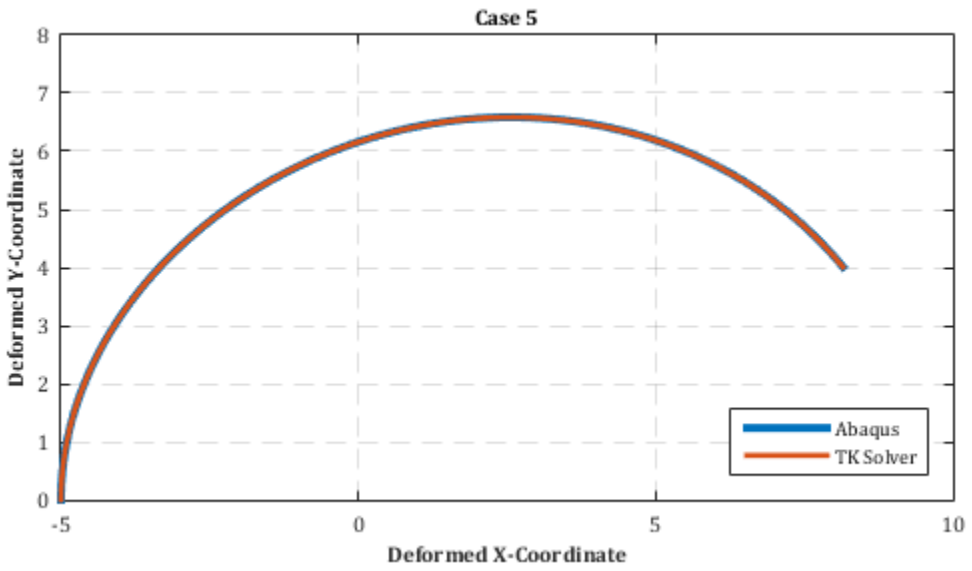

Figure 6-5 Case 5 Deformed Coordinates

Case 6

Case 6 featured a beam of the same geometry and loading as case 5. However, instead of the right end of the beam being free, there was a roller support present where the horizontal load was applied. The geometry and constraints are shown in Figure 6-6.

The moment equation for this case is the same as Case 5. However, due to the roller support at the right end, a Lagrange multiplier will be needed. A free body diagram of case 6 is shown in Figure 6-7.

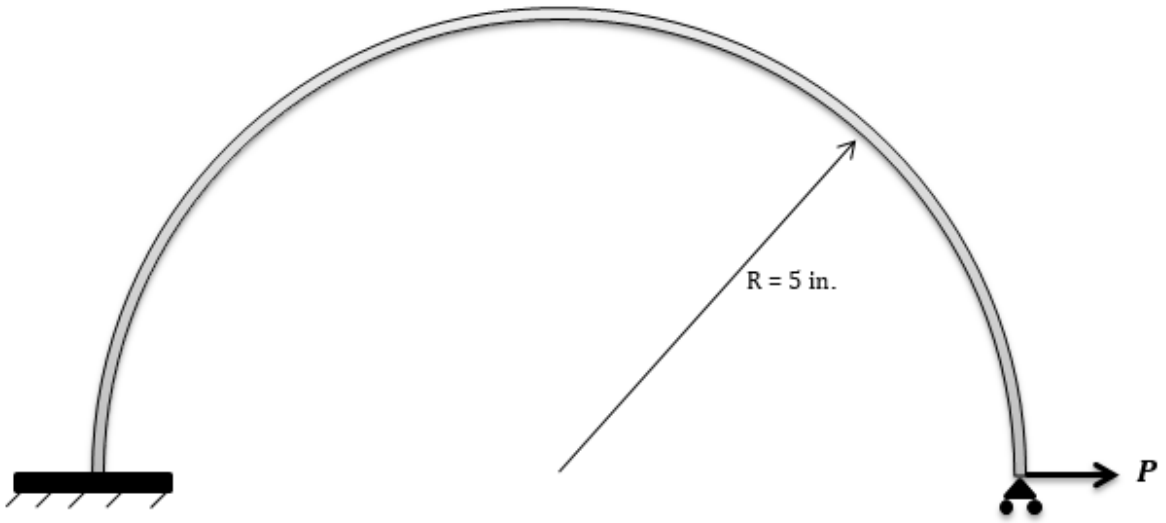

Figure 6-6 Case 6

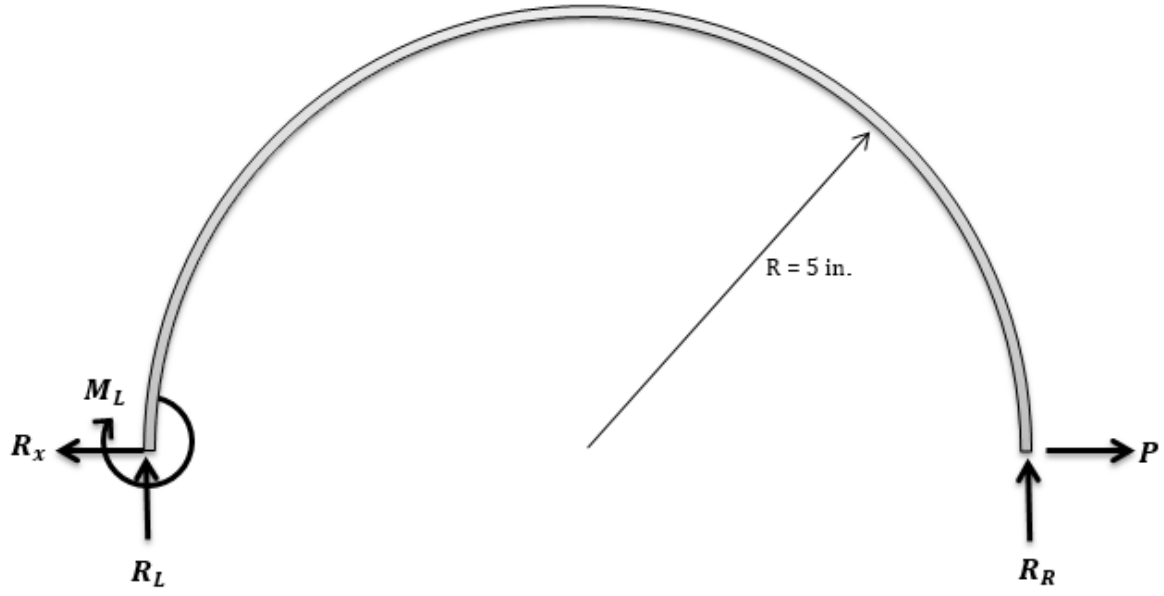

Figure 6-7 Case 6 Free Body Diagram

Analytical Methods

The form of Equation (2-3) will be used to account for the right end condition by including the Lagrange multiplier.

This problem was solved using finite element analysis and numerical integration in TK Solver. The finite element model is shown in Figure 6-8 below. The left end is fixed from rotation and translation about all three axes and the right end where the load is applied has been fixed in the *y*-direction in order to account for the roller support. The model included 787 nodes and 786 elements.

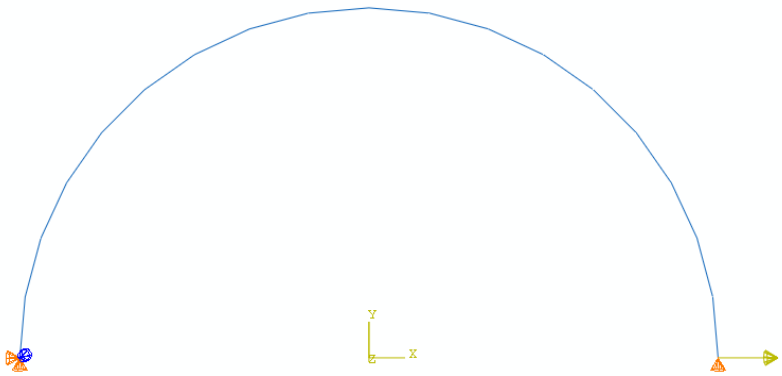

Figure 6-8 Case 6 Abaqus

The comparison between the FEA and the numerical integration are shown in the results section.

Results

The results of the FEA presented in Case 6 are shown in Figure 6-9. The color scale on the left hand side shows the values for horizontal displacement in inches. The deformed model is scaled 1:1 for viewing purposes.

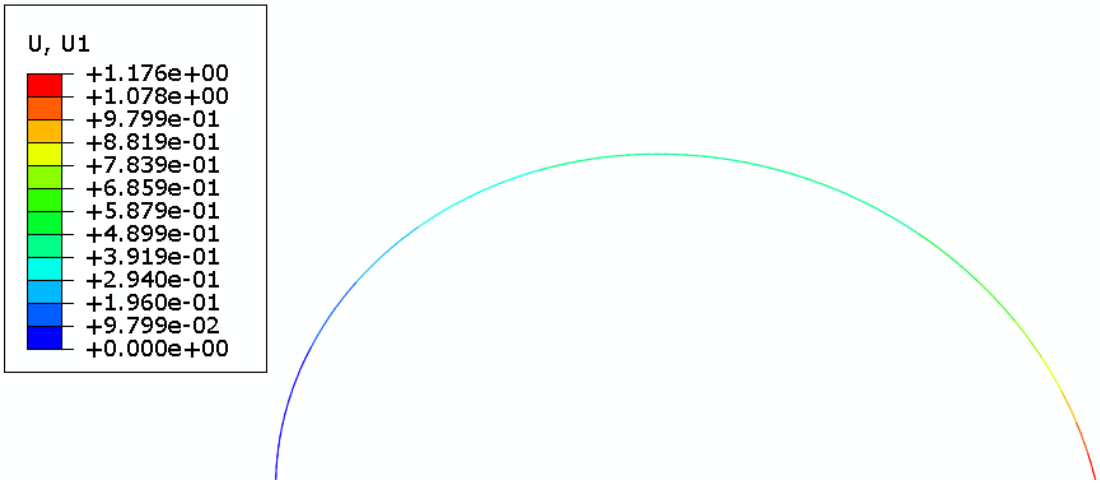

Figure 6-9 Case 6 Horizontal Displacement Abaqus

The graph presented in Figure 6-10 shows the deformed coordinates of the points analyzed on the beam for case 6.

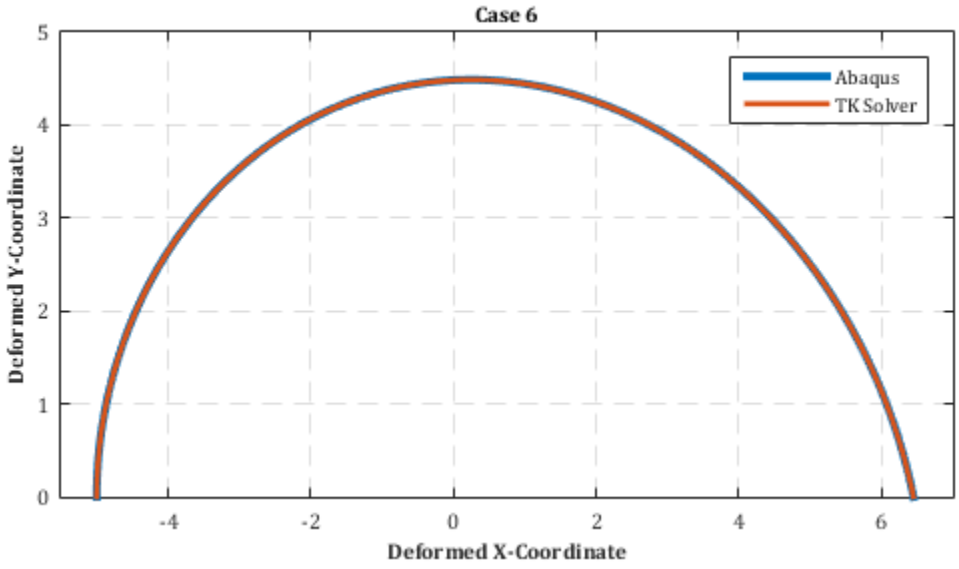

Figure 6-10 Case 6 Deformed Coordinates

Case 7

Case 7 featured the same geometry as Case 5 and Case 6. However, both ends of the beam were pinned, and a point load was applied at 45 degrees from the right end of the beam. The setup is shown in Figure 6-11.

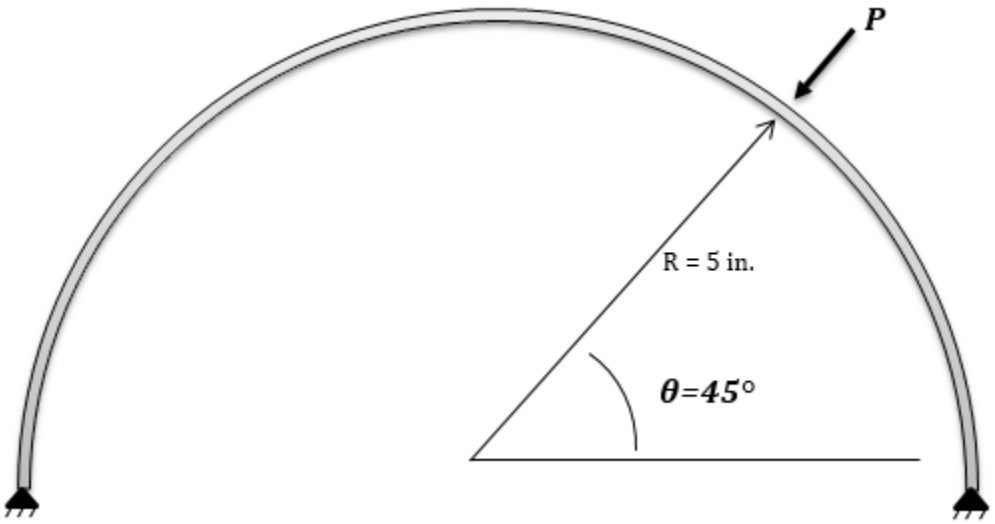

Figure 6-11 Case 7

The problem was solved using a finite element model created in Abaqus and numerically integrated using TK Solver. The model created in Abaqus is shown in Figure 6-12.

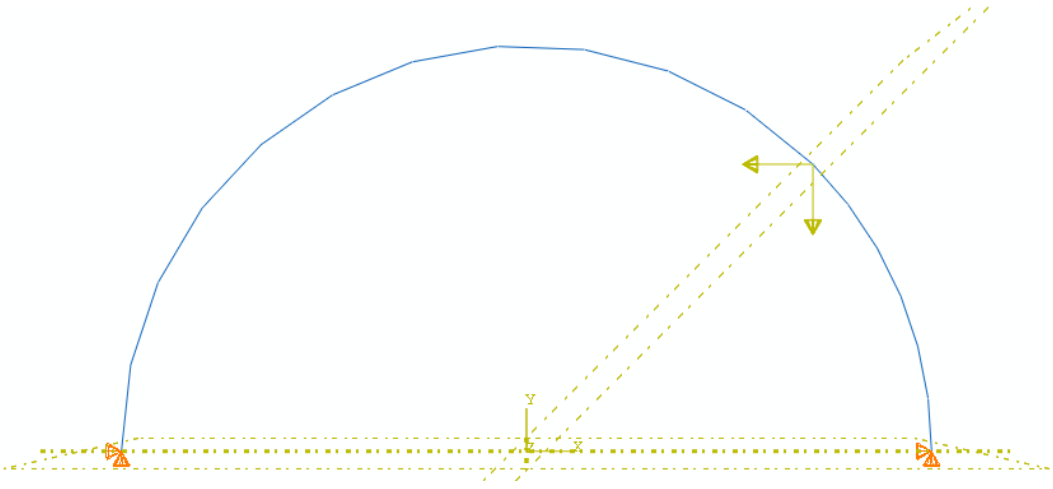

Figure 6-12 Case 7 Abaqus

In Figure 6-12, the dashed yellow lines are construction and datum planes used to partition the beam at 45 degrees so the force, *P*, could be applied at that location. The force P has been resolved into its *x* and *y*-components as shown in the figure. The model included 787 nodes and 786 elements. The comparison between the FEA and numerical solution are presented in the results section.

Results

Figures 6-13 and 6-14 show the results of the Abaqus model for case 7. Because the force was applied at 45 degrees for case 7, both the horizontal and vertical components of displacement are presented. The horizontal displacement, U1, is shown in Figure 6-13 and the vertical displacement, U2, is shown in Figure 6-14. The deformation in the Abaqus models have been magnified 5x for visual purposes. The colored scale in the upper left hand corner shows the value of displacement in units of inches.

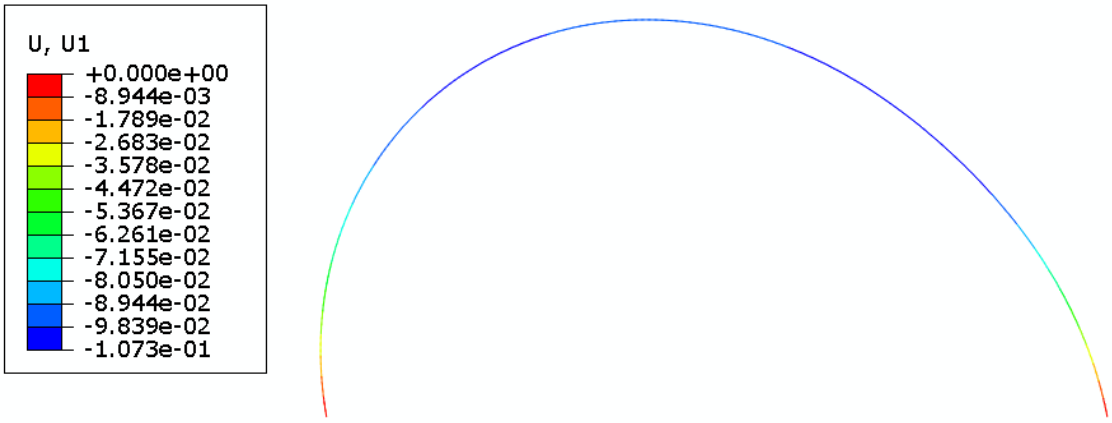

Figure 6-13 Case 7 Abaqus Horizontal Deflection

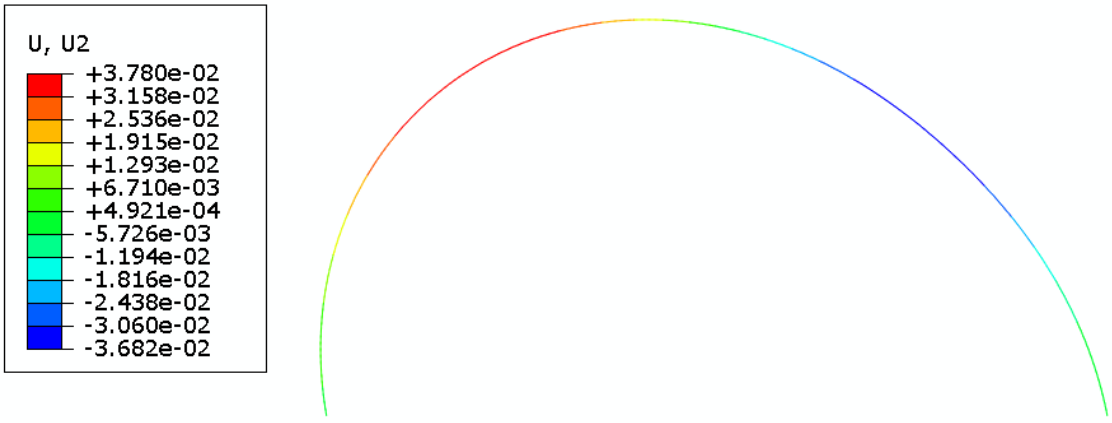

Figure 6-14 Case 7 Abaqus Vertical Deflection

Figure 6-15 presents the deformed coordinates of the curved beam for case 7.

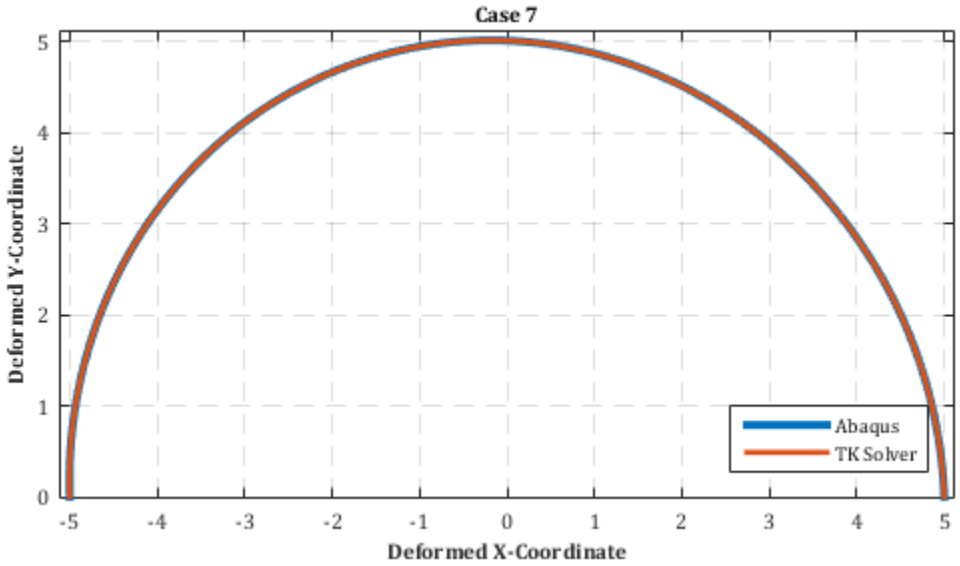

Figure 6-15 Case 7 Deformed Coordinates

Discussion

Even for cases of a more complicated geometry, the numerical and finite element solutions are very close and cannot be distinguished using standard graphing methods. Because the solutions agree so closely, confidence was built to proceed with the final orthodontic model. In the following chapter, the linear and non-linear models of the orthodontic force systems will be presented.

Chapter 7: Orthodontic Radial Model

Introduction

This chapter presents the final orthodontic model in detail. This problem was developed on the basis of a simple question: how much force does the orthodontic archwire apply to a patient's teeth during orthodontic treatment? The analytical solution to this problem was developed by Dr. Edwin Odom. It utilized Equation (2-3), and the theory introduced in Chapter 2 of this thesis. Recall that Castigliano's theorem, and the modified form of Equation (2-2) as well as the Crotti-Engesser method relate a point load to the displacement at that load. The goal was to solve the orthodontic force system for the unknowns: the fourteen reaction forces on the patient's teeth. This was done by using the displacements of each of the patient's teeth as the inputs and solving for the forces. The positions of the patient's teeth before and after treatment were used to obtain the displacements.

Two models were analyzed. The first featured a 316 stainless steel orthodontic archwire, and displacements of smaller magnitude. The stresses and strains involved with this model were in the linear regime. The second model featured a nickel-titanium archwire. The displacements were much larger in magnitude. There were some stresses and strains in the non-linear regime.

This chapter will introduce the geometry of the orthodontic models and explain the finite element models in detail. The results of the finite element analysis will be presented and compared to the numerical solution, which was developed using the closed-form solution aside from utilizing numerical integration.

Radial Orthodontic Model

The locations where the fourteen reaction forces occurred were designated as *F1-F14*, as demonstrated in Figure 7-1. It should be noted that some of the figures presented in this chapter do not follow the same format as the rest of the figures in this thesis. These figures were from a paper submitted for publication in the *American Journal of Orthodontics and Dentofacial Orthopedics*.

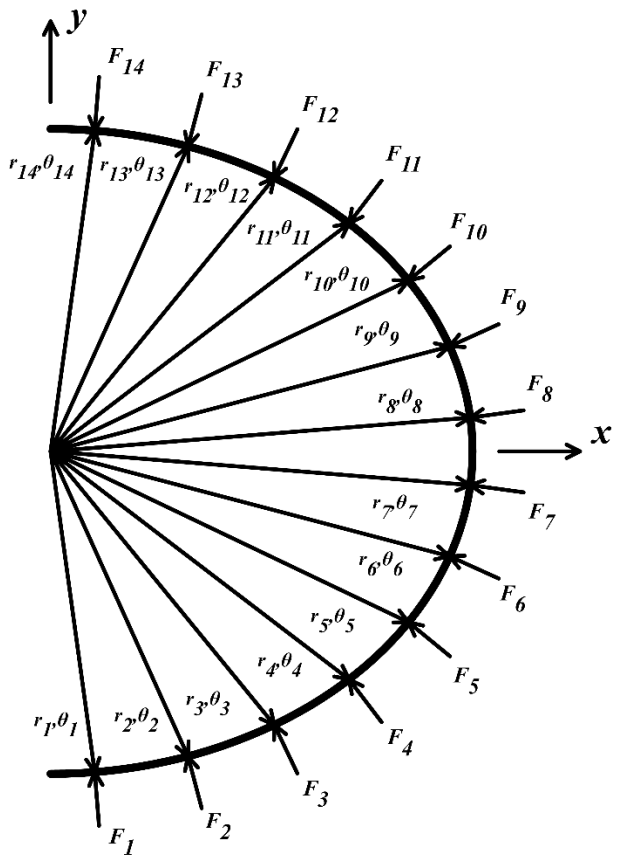

Figure 7-1 Orthodontic Force System

Analytical Methods

The basics of the closed-form solution will be presented. Further derivation of the closed-form solution is beyond the scope of this thesis. The closed-form solution and numerical integration program were developed by Dr. Edwin Odom.

The moment equation was established by calculating the vector $\boldsymbol{r}$ between an applied load and the point of interest. Refer to Figure 7-2 on the following page. The other depicted vectors, $\boldsymbol{r_i}$ and $\boldsymbol{r_\theta}$, are used to calculate the length of $\boldsymbol{r}$ as shown below.

$$\boldsymbol{r} = \boldsymbol{r_i} - \boldsymbol{r_\theta}$$

Consider the vector $\boldsymbol{r}$ as the moment arm and the force F_i as the applied load. The moment at the point of interest is calculated using a cross product between $\boldsymbol{r}$ and F_i. The moment equation is a function of θ and is shown below.

$$M(\theta) = \sum_{1}^{14} (\boldsymbol{r} \times F_i) H(\theta, \theta_i)$$

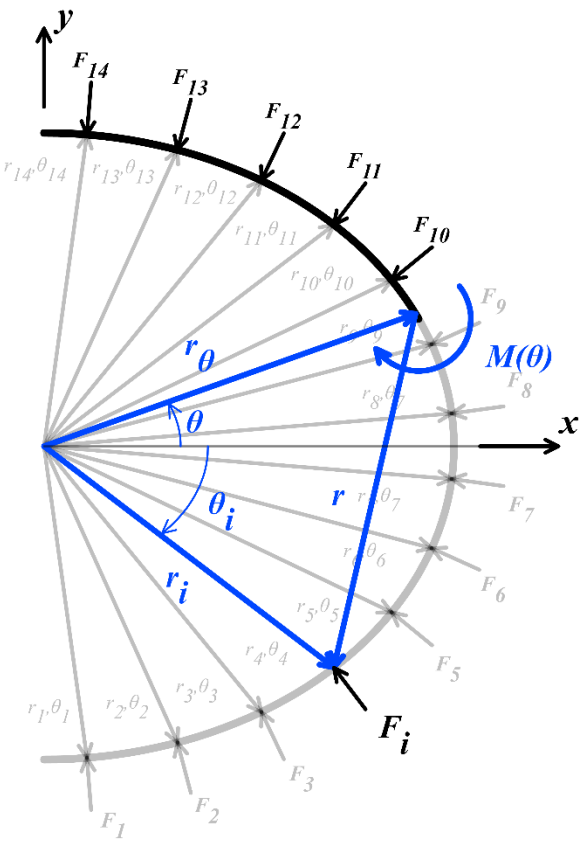

Figure 7-2 Free Body Diagram Orthodontic Model

The partial derivative of the moment with respect to the force at the point of interest is shown below. It is needed for one of the governing equations.

$$\frac{\partial M(\theta)}{\partial F_k} = (r_k - r_\theta) * H(\theta, \theta_k)$$

The partial derivative and the moment equation were used in the modified form of Castigliano's theorem below. The complementary energy was used due to the inelastic behavior of the model.

$$\delta_k = \int \frac{\partial U^*}{\partial M} \frac{\partial M}{\partial F_k} ds + \lambda_1 \frac{\partial g_1}{\partial F_k} + \lambda_2 \frac{\partial g_2}{\partial F_k} + \lambda_3 \frac{\partial g_3}{\partial F_k} \qquad (1)$$

The Lagrange multipliers associated with the modified form of Castigliano's theorem, Eq. (2-3), must be determined. The equations of equilibrium will be used and are presented below.

$$g_1 = \sum F_x = 0 \tag{2}$$

$$g_2 = \sum F_y = 0 \tag{3}$$

$$g_3 = \sum M_z = 0 \tag{4}$$

After the governing equations were established, the problem featured 17 equations and 17 unknowns. The system of equations was solved numerically in a TK Solver program.

Finite Element Analysis

The finite element analysis capabilities of Abaqus were used to verify the analytical solutions for the orthodontic force system. Locations *F1–F14* were established by creating datum planes at angles θ_1–θ_{14} and partitioning the wire model at the plane-model intersections. There were boundary conditions at locations *F1*, *F5*, and *F14*. *F1* and *F14* were fixed only in the *y*-direction, to allow for sliding in the *x*-direction. *F5* was fixed in both the *x* and *y*-direction.

The finite element model setup was slightly different than the numerical setup. Instead of the displacements being inputs to the finite element model, the inputs were the reaction forces from the numerical model. Figure 7-3 shows a visual result of the numerical solution. The magnitude and direction of the calculated reaction forces are shown. These reaction forces were the inputs to the finite element models. The displacements produced from the FEA were compared to the actual displacements of the patient's teeth.

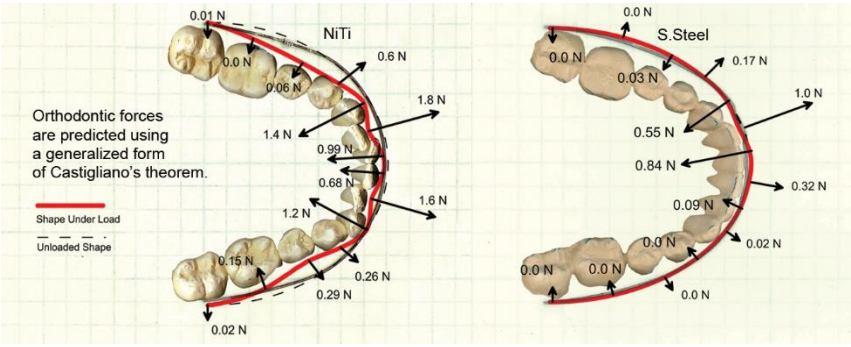

Figure 7-3 Nonlinear Solution (Left) and Linear Solution (Right)

Linear Model

The linear model was constructed first. The linear model was used to represent the later part of orthodontic treatment. Toward the end of treatment, the teeth are close to their desired position. The later movements of the teeth are rather small. Stiffer, steel archwires are used. Additionally, because the distance the teeth move is small, the wire remains in elastic deformation and bending. For the linear model, the Young's modulus was 2.8E7 psi. The profile was rectangular: 0.019 inches parallel and 0.025 inches perpendicular to the neutral axis. The model was globally seeded using an approximate global size of 0.005. The element type was a 2-node linear, planar beam. The model included 941 nodes and 940 elements. The setup is shown in Figure 7-4.

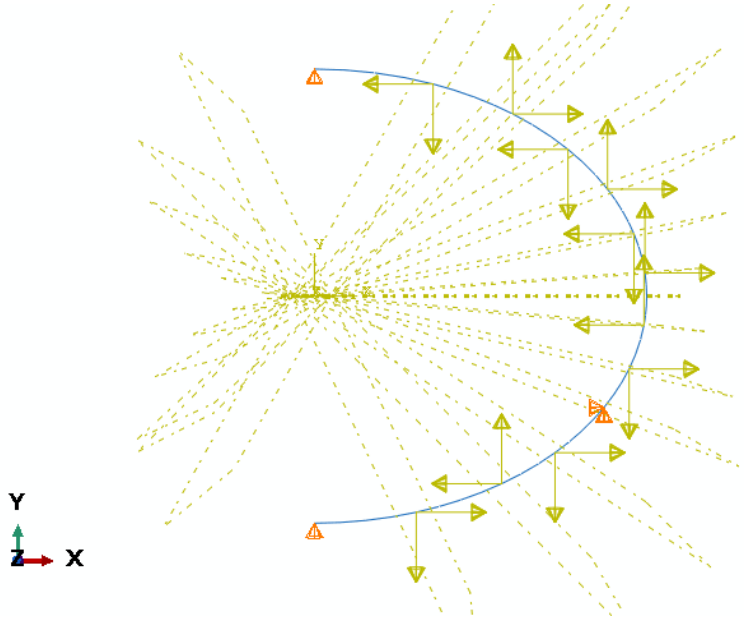

Figure 7-4 Abaqus Linear Final Model

In Figure 7-4, it can be seen that locations *F1* and *F14* are fixed in the *y*-direction as stated, and *F5* is fixed in both the *x* and *y*-direction. The dashed yellow lines are datum planes used to partition the wire at locations θ_1–θ_{14}. The analysis was run to solve for displacement. The results of the analysis and a comparison between the FEA and numerical model are presented in the results section of this chapter.

Nonlinear Model

For the non-linear nickel-titanium material, stress-strain data [12] was input for the plastic analysis in Abaqus. The elastic modulus for the NiTi material was 9.1×10^6 psi for the linear portion of the stress-strain curve. The NLGEOM option for the non-linear model step was activated. The geometrical setup was the same as the linear model and is represented by Figure 7-4.

The predicted shape of the wire obtained from the FEA model was compared to the analytical solution. The results of the FEA and the comparison are presented in the results section.

Results

The results of the finite element analysis are presented below. Both the displacement in the horizontal, U1, and vertical, U2 directions are presented. The colored scales in the upper left-hand corner of the following images have units of inches. The deformation in the models themselves has been magnified 100x for visual purposes.

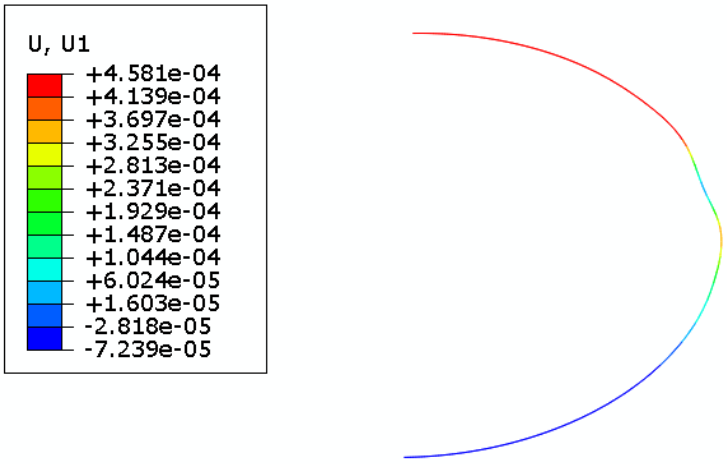

Figure 7-5 Abaqus Horizontal Deflection Linear Case

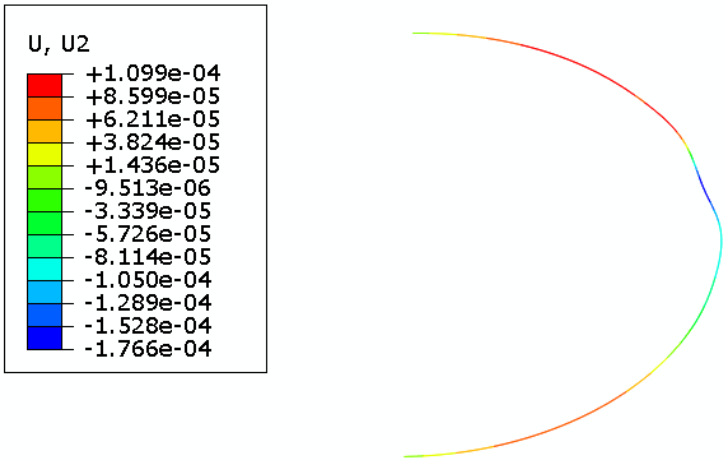

Figure 7-6 Abaqus Vertical Displacement Linear Case

The deformed coordinates of the archwire were taken from the numerical solution and FEA model. When plotted on the same chart, the graphs overlapped and distinguishing between the two was very difficult considering the extremely small magnitude of the displacements. The original and deformed shape of the wire can be seen in Figure 7-7.

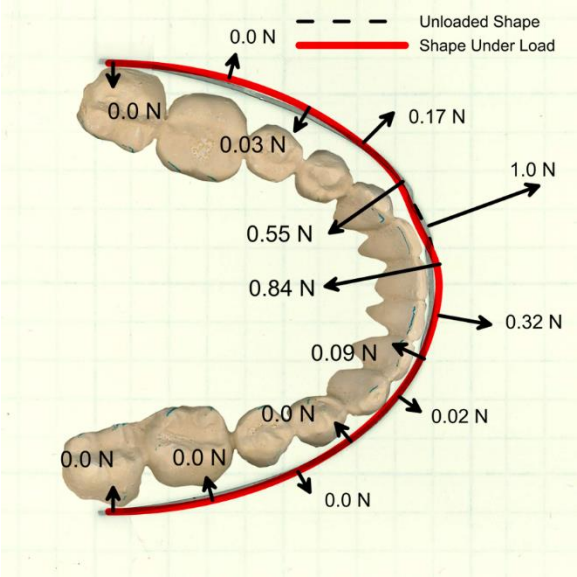

Figure 7-7 Original and Deformed Shape Linear Case

At the location of largest displacement, the numerical solution produced a radial displacement of .00018 inches, and the FEA produced a radial displacement of .00023 inches.

The results of the non-linear case are shown in Figures 7-8 and 7-9. The deformation in the models was not magnified. The displacements can easily be distinguished using a 1:1 scale.

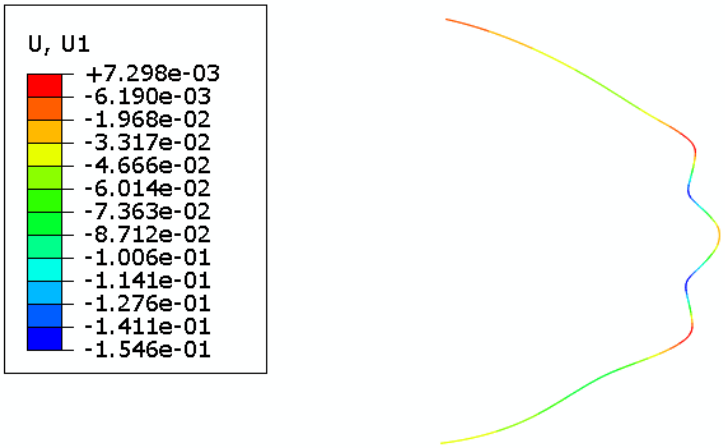

Figure 7-8 Abaqus Horizontal Displacement Non-Linear Case

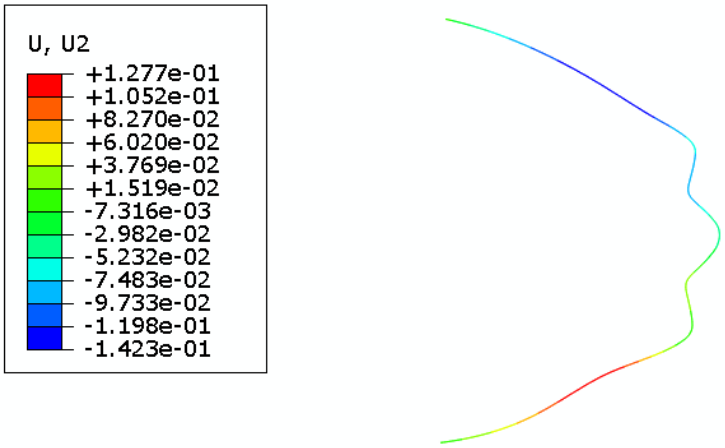

Figure 7-9 Abaqus Vertical Displacement Non-Linear Case

The deformed coordinates of the archwire from both the numerical solution and FEA model were graphed for comparison. The graph is shown in Figure 7-7.

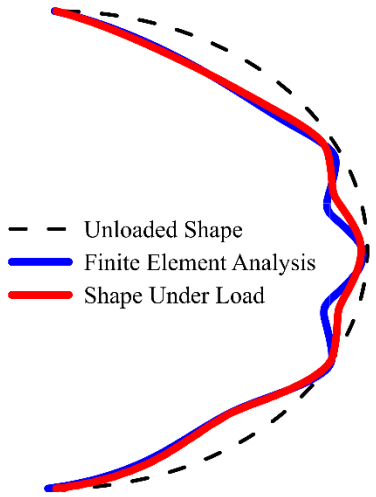

Figure 7-10 Non-Linear Final Orthodontic Model

Discussion

The results for the linear model will be discussed first. The linear model is for circumstances when the patient is toward the end of treatment. The wire is much stiffer, and the displacements are smaller. Because the displacements are small, the wire remains in the linear regime. At the point of largest deflection, the answers differed by over 25%. This may seem like a lot, however, the displacements had five significant digits. If one were to round to the fourth decimal place, then the calculated displacements are identical.

The non-linear model featured the NiTi wire. This model was to represent the beginning of treatment when the teeth may need to significantly change position, and the displacements are much larger, on the order of 0.1 inches compared to .0001 for the linear model. Considering the complicated analysis which features methods that have not been proven, the fact that the displaced curves of Figure 7-7 match so closely indicate the proposed solution to the orthodontic force system is accurate.

Chapter 8: Discussion and Conclusion

The base cases which were developed to test the accuracy of the finite element models and the closed-form solution were very successful. The methods used to develop the closed-form solutions for the base cases were extensive. There are less extensive approaches to solving these problems such as the double integration method and even published closed-form solutions for some of the early base cases. However, using the modified form of Castigliano's theorem on the simple base cases with published solutions allowed the validation of the approach. Then the modified form of Castigliano's theorem and the Crotti-Engesser method could be applied with confidence to a much more complex model like the orthodontic force system. In the case of the orthodontics, using another approach to solve the problem would not be quicker or more efficient. The simple base cases were needed to validate the analytical approach such that it could be applied to a case where it was needed.

In addition to the base cases, the final model proved to be a success. The results presented in all previous chapters of this thesis support the idea that the modified version of Castigliano's theorem including the use of Lagrange multipliers is accurate when applied to simple cases, complex cases, and even cases including inelastic stresses and strains. Because of the closeness in results of the final model, it can be said that the modified form of Castigliano's theorem and the Crotti-Engesser method can be successfully applied to statically indeterminate problems and problems involving non-linear material behavior.

The ideas and methods presented in this thesis may be of interest to the orthodontic industry. Forces on a single tooth have been determined based on experimentation. But relating the movement of each tooth to a system of forces has not been done.

The real benefit of this research is the new way to solve mechanics problems, particularly those that are statically-indeterminate or involve non-linear material behavior. This method has already been applied to find the deflections in tractor trailer beds and large stepped shafts under complicated loading conditions.

References

[1] P. Orthodontics, "Parts & Appliances," 2019. [Online]. Available: http://www.pawleyortho.com/parts-of-braces.php. [Accessed 22 April 2019].

[2] Indiamart, "Orthodontic Archwires," 1996-2018. [Online]. Available: https://www.indiamart.com/stm-meditech/orthodontic-wires.html. [Accessed 22 April 2019].

[3] "Purdue University," 2012. [Online]. [Accessed February 2019].

[4] Boresi and Schmidt, Advanced Mechanics of Materials, Wiley, 2002.

[5] F. D. Ju, "On the Constraints of Castigliano's Theorem," *Journal of the Franklin Institiute,* vol. 292, no. 4, pp. 257-264, 1971.

[6] W. Steiner, "The use of Castigliano's theorem in Coulomb friction problems," *Springer Vienna,* 2014.

[7] C. Egelhoff and E. Odom, On calculating the slope and defleciton of a stepepd and tapered shaft, 2014.

[8] E. Odom and C. J. Egelhoff, Teaching deflection of stepped shafts: Castigliano's theorem, dummy loads, heaviside step functions and numerical integration, 2011.

[9] A. Meghdari, "A Variational Approach for Modeling Flexibility Effects in Manipulator Arms," *Robotica,* vol. 9, no. 2, pp. 213-217, 1991.

[10] Shigley and Mischke, Mechanical Engineering Design, |McGraw Hill, 1989.

[11] A. Higdon, E. H. Ohlsen and W. B. Stiles, Mechanics of Materials, John Wiley & Sons, Inc., 1962.

[12] J. Fercec, M. Kos, M. Bruncko, I. Anzel, B. Glisic, E. Markovic and R. Rudolf, "COMPARISON OF NiTi ORTHODONTIC ARCHWIRES AND A DETERMINATION OF THE CHARACTERISTIC PROPERTIES," *Materials and Technology,* 2014.